Fall 1-31-2014

# Analysis of transport properties in a zaz graphene nanoribbon junction using various dopants

Natasha Parikh
*New Jersey Institute of Technology*

# Copyright Warning & Restrictions

The copyright law of the United States (Title 17, United States Code) governs the making of photocopies or other reproductions of copyrighted material.

Under certain conditions specified in the law, libraries and archives are authorized to furnish a photocopy or other reproduction. One of these specified conditions is that the photocopy or reproduction is not to be "used for any purpose other than private study, scholarship, or research." If a, user makes a request for, or later uses, a photocopy or reproduction for purposes in excess of "fair use" that user may be liable for copyright infringement,

This institution reserves the right to refuse to accept a copying order if, in its judgment, fulfillment of the order would involve violation of copyright law.

Please Note: The author retains the copyright while the New Jersey Institute of Technology reserves the right to distribute this thesis or dissertation

Printing note: If you do not wish to print this page, then select "Pages from: first page # to: last page #" on the print dialog screen

## ABSTRACT

### ANALYSIS OF TRANSPORT PROPERTIES OF A ZAZ GRAPHENE NANORIBBON JUNCTION USING VARIOUS DOPANTS

**by**
**Natasha Parikh**

A 12 atom wide ZAZ Graphene Junction was simulated and its transport properties were analyzed. I-V curves, calculated by nonequilibrium Greens function method combined with the density functional theory under external bias, showed varying semiconducting characteristics. Further, the width of the junction also showed significant effects in the determination of the semiconducting nature. A theoretical study was performed on the semiconducting characteristics by analyzing the I-V curve and transport coefficients in the junction.

# ANALYSIS OF TRANSPORT PROPERTIES IN A ZAZ GRAPHENE NANORIBBON JUNCTION USING VARIOUS DOPANTS

**by**
**Natasha Parikh**

**A Thesis**
**Submitted to the Faculty of**
**New Jersey Institute of Technology**
**in Partial Fulfillment of the Requirements for the Degree of**
**Master of Science in Materials Science and Engineering**

**Interdisciplinary Program in Materials Science and Engineering**

**January 2014**

**APPROVAL PAGE**

**ANALYSIS OF TRANSPORT PROPERTIES IN A ZAZ GRAPHENE NANORIBBON JUNCTION USING VARIOUS DOPANTS**

**Natasha Parikh**

---

Dr. N. M. Ravindra, Thesis Advisor — Date
Director of Material Science and Engineering Program, NJIT

---

Dr. Keun H. Ahn, Committee Member — Date
Associate Professor of Physics, NJIT

---

Dr. Tao Zhou, Committee Member — Date
Associate Professor of Physics, NJIT

---

Dr. Halina Opyrchal, Committee Member — Date
Senior University Lecturer of Physics, NJIT

## BIOGRAPHICAL SKETCH

**Author:** Natasha Parikh

**Degree:** Master of Science

**Date:** January 2014

**Undergraduate and Graduate Education:**

- Master of Science in Materials Science and Engineering,
  New Jersey Institute of Technology, Newark, NJ, 2014

- Bachelor of Arts in Physics and Biological Sciences,
  Rutgers, the State University of New Jersey, New Brunswick, NJ, 2012

**Major:** Materials Science and Engineering

## ACKNOWLEDGMENTS

I would like to express my gratitude to my supervisor Dr. N.M Ravindra for the useful comments, remarks and engagement throughout the learning process of this Masters' thesis. Furthermore, I would like to thank Vijay Kasi Somayajula for introducing me to the topic as well for the support. I thank Dr. Tao Zhou, Dr. Ken Ahn and Dr. Halina Opyrchal for serving on my thesis Committee. I would like to thank my loved ones, who have supported me throughout the entire process, both by keeping me harmonious and helping me in putting pieces together.

## TABLE OF CONTENTS

**TABLE OF CONTENTS**
**(Continued)**

## LIST OF FIGURES

## LIST OF FIGURES
## (Continued)

## LIST OF FIGURES
## (Continued)

# CHAPTER 1

# INTRODUCTION

## 1.1 Graphene: The New Carbon

Carbon (chemical symbol C, atomic mass 12.07amu) (Figure 1.1a) is a widely distributed element in nature. It is found abundantly in the sun, stars, comets and the atmospheres of the planet. Carbon can form up to four bonds; it can bond with itself endlessly and with most other elements in many different shapes, making it a significant part of the construction for many kinds of complex molecules.[1]

Two allotropes of carbon are commonly used, diamond and graphite (Figure 1.1b). The bonding structures of diamond and graphite contribute to the properties individually. In diamond, all the *p*-orbitals are used forming a $sp^3$ bonding whereas, in graphite, only two orbitals are occupied allowing the unpaired bond for the transport of electrons. Each carbon atom in graphene possesses $sp^2$ hybridization i.e., each carbon atom is connected to three other carbon atoms via covalent bonds with a bond length of 1.42Å and an angle of 120° between each bonded pair. This makes graphite a better conductor than diamond. Graphite consists of many layers of 2D carbon lattices (Figure 1.1c) stacked on top of each other and held via Van der Waals forces. A single layer of graphite, where carbon atoms are arranged in a honeycomb lattice, is known as graphene (Figure 1.1c).

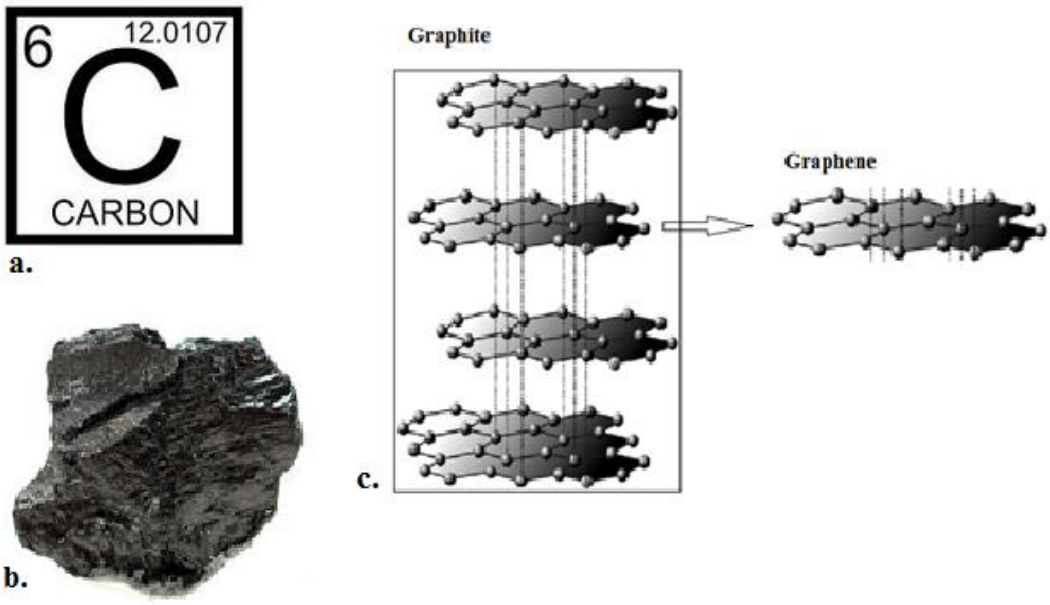


**Figure 1.1** (a) Chemical representation of Carbon (b) Graphite ore (c) Structure of Graphite and a single layer Graphene.[2]

Theoretical work on graphene was done specifically to study the other allotropes. The first study was done by Wallace in 1947, who calculated the band structure of graphene.[3] Further, the peculiar Landau levels were known by McClure in 1957 and the relativistic Hofstadter butterfly by Ramal in 1985.[3] Later in 1991, the invention of carbon nanotubes by Iijima boosted the theoretical research on graphene.[3] Prior to the invention of carbon nanotubes, there were a few experimental papers on graphene growth via various methods like intercalation of graphite (Shioyama, 2001), free standing (Boehm, 1962), epitaxial as well as graphene grown on metals (Bommel, 1975; Land 1992; Itoh 1991)[3]. With all the various discoveries, the electronic properties of graphene were not studied until 2004, when Berger and Novoselov were able to access the electronic properties with contact of graphene flakes[3] (Figure 1.2).

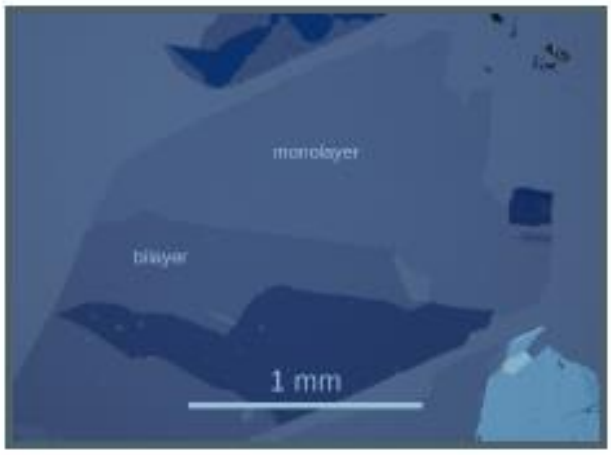


**Figure 1.2** An optical image of Graphene flake obtained by exfoliation of graphite.[3]

The specific lattice structure of graphene possesses a number of unique electronic properties making it an interesting material for theorists, experimentalists and engineers. Utilization of graphene, as a fundamental block of electronic devices, requires development of new theoretical methods for understanding the current propagations in graphene constriction.[4]

## 1.2 Graphene Synthesis

The discovery of graphene by mechanical exfoliation, called the 'Scotch tape method' led to serious attempts towards the production of top quality graphene.[5] Graphene was first exfoliated mechanically from graphite in 2004.[6] The importance of high quality graphene cannot be emphasized enough; however, electron transport has shown that defects play an important role in hindering the transport properties of electrons (holes).[7] The two synthesizing methods for the large scale manufacture of graphene are chemical vapor deposition (CVD) and silicon carbide (SiC) desorption method.

Graphene can be synthesized by sublimation of silicon from SiC at high temperature (1200°C) in high vacuum.[5] The major advantage of this method is that the SiC provides an insulating substrate and no transfer of the graphene layer is needed. Yet, the disadvantage of this method outweighs its advantages; the high temperature is cost-ineffective making it unsuitable for large scale manufacturing.[8] Also, the crystal growth face alters the properties of graphene. Graphene, grown on Si-terminated face, has poor homogeneity and is subjected to unintentional doping.[7] Conversely, graphene grown on C-terminated SiC has higher mobility and is often called 'turbostatic' due to the rotational disorder.[7]

Unlike the SiC method, the graphene produced via CVD method needs to be transferred to a substrate making it difficult to maintain the quality of graphene. Yet, CVD synthesized graphene has a larger grain size.[7] More research is being done on various methods for synthesis of graphene. The methods include direct chemical synthesis, ion implantation, crystal sonification and lastly unzipping carbon nanotubes to form graphene sheets.[9]

Graphene and few-layer graphene have been grown by CVD from carbon containing gases on catalytic metal surfaces and/by surface segregation of C dissolved in the bulk of such metals.[7] Growing graphene with CVD is a very attractive solution, since it is compatible with the existing semiconductor industry.[9] Graphene has been grown via CVD process on metal substrates such as Nickel (Ni) and Copper (Cu).

### 1.2.1 Synthesis of Graphene on Nickel (Ni)

Polycrystalline Ni films are annealed in $Ar/H_2$ atmosphere at 900-1000°C to increase grain size and are then exposed to $H_2/CH_4$ gas mixture.[10] In this step, the hydrocarbon decomposes and dissolves in Ni to form a solid solution. Lastly, the samples are cooled in argon gas. Ni has high carbon solubility at elevated temperatures, and the solubility decreases as temperature is reduced. During the cooling process, the carbon atoms diffuse out from the Ni-C solid solution and precipitate on the Ni surface to form graphene films (Figure 1.3a). Since Ni (111) has a lattice similar to the densely packed hexagonal lattice of graphene, (Figure 1.3b), they also have similar lattice constants, and hence Ni surface serves as an excellent lattice matched substrate for graphene growth.[11]

The growth of graphene on Ni is based on carbon segregation and precipitation process; different segregation behavior is produced by different cooling rates, which affect the thickness and quality of graphene films.[12] Medium cooling rates lead to optimal carbon segregation and produce few layers.[12] Graphene films, grown on Ni, are usually continuous with monolayer and few layer regions. Annealing of Ni substrates, at elevated temperatures in hydrogen atmosphere, not only increases the single-crystalline Ni grain size but also eliminates certain impurities in Ni, thereby improving the graphene quality. Furthermore, the graphene thickness can also be affected due to the amount of carbon dissolved in the Ni films during the growth time.

After synthesis, the graphene can be transferred to other insulator substrates for further characterization and applications. Figure 1.3c shows the selected area electron diffraction pattern of graphene film along the [001] direction, which confirms the graphene lattice structure shown. After transfer to insulator substrates, the geometry can

be retained as shown in Figure 1.3d. Under optimal growth parameters, graphene growth is only limited by the Ni catalyst. Lastly, Figures 1.3e and 1.3f show the wafer-scale graphene synthesis and transfer of graphene to a flexible transparent substrate, respectively.

Though polycrystalline Ni is a good substrate, the percentage and size of graphene monolayer are still limited. Researchers have hence tried other metal substrates for graphene synthesis.

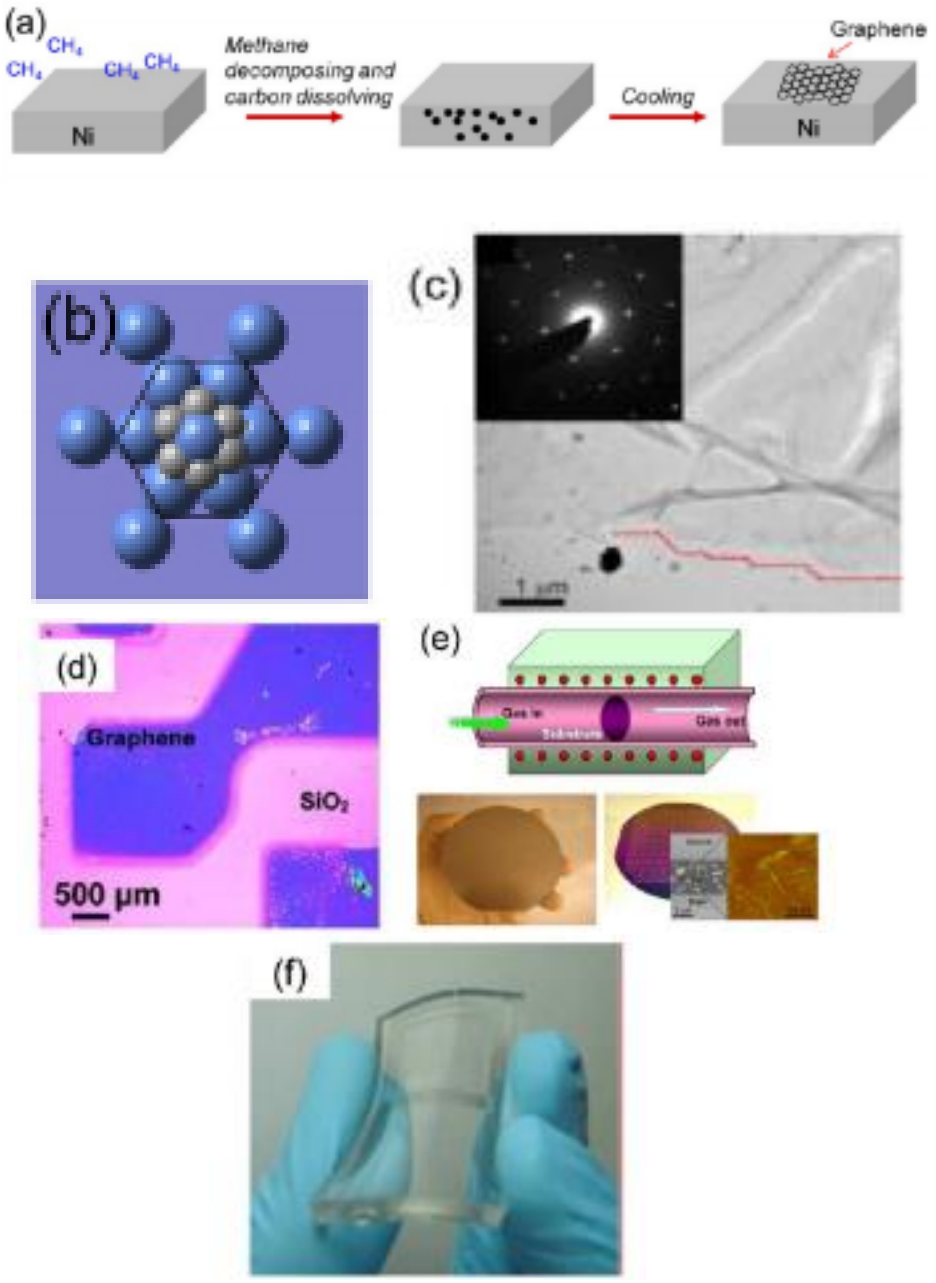


**Figure 1.3** (a) Graphene formation on Nickel; (b) Graphene atoms on Ni (111) lattice; (c) Low magnification TEM image of graphene edges; (d) Optical image of graphene transferred from the Ni surface to $SiO_2$/Si substrate; (e) Full-wafer scale deposition of graphene layers on polycrystalline Ni; (f) Transparent and flexible graphene films on PDMS substrate.[10]

### 1.2.2 Synthesis of Graphene on Copper (Cu)

Graphene films are grown on 25μm thick Cu foils in a hot wall furnace.[13] The Cu foil is first annealed in hydrogen atmosphere at 1000°C and a mixture of $H_2/CH_4$ is introduced into the system to initiate graphene growth. After a continuous graphene layer is formed on the Cu foil, the system is cooled to room temperature. Figure 1.4a shows an SEM image of graphene on Cu substrate, indicating the Cu grains with contrast. The Cu surface steps are formed during thermal annealing and the darker flakes indicate multiple-layer graphene (Figure 1.4b).[10] The graphene wrinkles, in Figure 1.4(b), originate from different thermal expansion coefficient of graphene and Cu. They go across the Cu grain boundaries indicating that the graphene film is continuous.

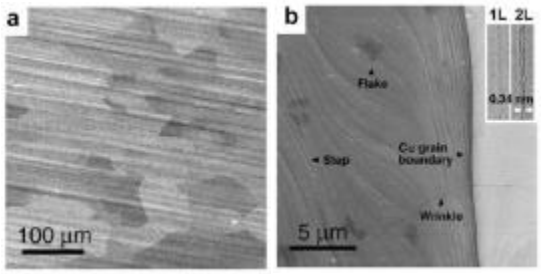


**Figure 1.4** (a) SEM image of graphene on copper foil (b) High-resolution SEM image of graphene on Cu.[10]

### 1.2.3 Transfer of Graphene films

In order to facilitate the applications of graphene for electronic applications, we need to separate the graphene from the catalytic metal substrate. Figure 1.5a shows the transfer process of graphene. Graphene is first coated with a thin layer of polymethyl methacrylate (PMMA) and baked at 120°C to evaporate the solvent.[10] The metal layer is then removed by Ni or Cu etchant, leaving behind the PMMA graphene film. The film is then cleaned by deionized water and then transferred onto the target substrate. After the

evaporation of water vapor, the PMMA is removed by acetone, leaving graphene film on top of the target substrate. Figure 1.5b shows a graphene wafer transferred from the substrate onto glass and polyethylene terephthalate (PET) films.

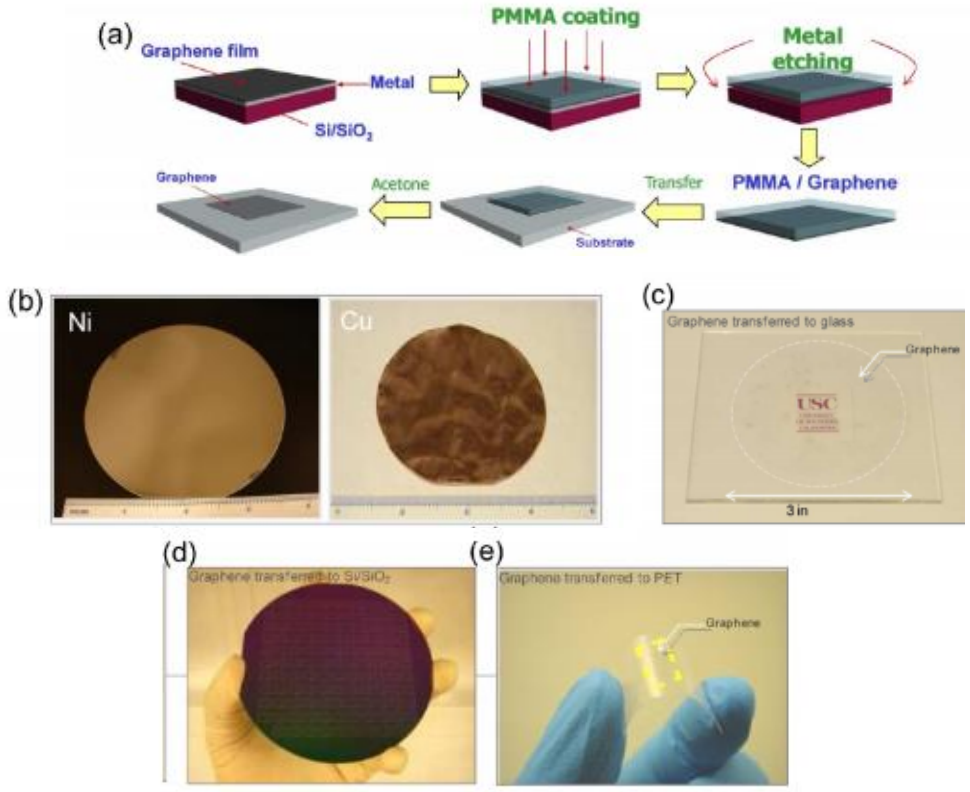


**Figure 1.5** (a). Transfer process; (b). Wafer-scale synthesis of graphene; (c). Graphene films transferred onto glass wafer; (d). $Si/SiO_2$ with device patterned; (e). PET film.[10]

### 1.2.4 Synthesis of Graphene Junction

Graphene junctions, with smooth armchair and zigzag edges, are difficult to produce by conventional methods such as mechanical exfoliation, chemical exfoliation or lithography etching.[14] The conventional methods can only produce rough edges. Recently, Dresselhaus reported an edge reconstruction of graphene by Joule heating in a TEM-STM

(Figure1.6b) system.[15] An individual nanoribbon sample is attached to the sample holder at one end and to the STM tip at the other end; these ends also serve as the two electrodes. The structural transformation in the growth of graphene from armchair to zig-zag is mainly attributed to the vaporization of carbon edges that reconstruct at high temperatures, in which resistive Joule heating and preferred current flow play an important role. This means that, by controlling the flow of current, a perfectly smooth edged ribbon can be synthesized making graphene-based electronics possible.[16]

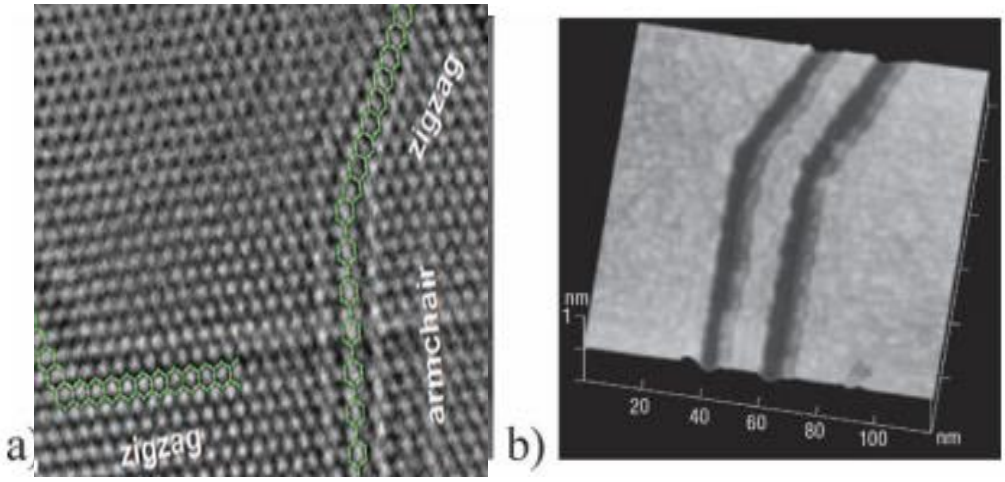


**Figure 1.6** (a) High-magnification image of the annealed sample showing that well-defined zigzag armchair and zigzag-zigzag edges are formed. (b) STM image of an 8 nm wide bent junction connecting an armchair and a zigzag graphene nanoribbon, which was carved by STM tips.[14]
.

### 1.2.5 Doping in Graphene

The doping of graphene can be roughly classified into two categories - electrical and chemical. Electrical doping involves changing gate voltages of graphene devices and chemical doping uses chemical routes such as substitutional or interstitial. This thesis discusses chemical doping and the importance of doping sites by changing the dopant.

Chemical doping is a common approach to tailor the electronic properties of

semiconductors. Doping of graphene can cause its electronic properties to alter leading to a metal-semiconductor transition. The two means of doping graphene are interstitial and substitutional. In interstitial doping, the dopant atoms or molecules are introduced as adatoms or admolecules on the surface of graphene, whereas in substitutional doping, the dopant atoms are replaced in the carbon lattice forming a bond in the lattice of graphene.[16] Doping graphene results in the formation of n or p-type semiconductors depending on the kind of dopant. If the dopant is an electron donor, it causes the Fermi level to shift up resulting in n-type behavior of graphene. Furthermore, if the dopant is an electron acceptor, it causes the Fermi level to shift down resulting in a p-type behavior of graphene (Figure 1.7).[16]

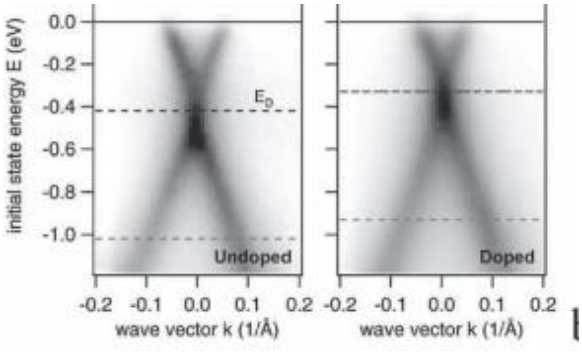


**Figure 1.7** Band structure of graphene before and after doping. The image shows shift towards the Fermi level.[16]

Graphene nanoribbons (GNR) can be made into a p- and n- type semiconductor by doping with boron (B) and nitrogen (N) respectively. In theory, GNR p-n junction is formed by doping GNR with B and N in different regions. However, experimentally, doping graphene with both these elements is very difficult due to the dopants reacting with each other.[17] Hence, most experimental studies use GNR doped by only one

element. N-doped graphene was synthesized by Wei et al., Wang and B-doped Graphene was realized by Endo.[17]

Many researchers have demonstrated interstitial doping of graphene by gas, metal and organic molecules.[16] The various gases and metals used are $NO_2$, $NH_3$, An-$CH_3$, Na-$NH_2$, F4-TCNQ, TPa, TCNE and others.[16] Doping in graphene is hence possible by electrons or holes in high concentration without deterioration of its mobility. Interstitial doping is highly sensitive due to most of the conducting channel being exposed to surface absorbates and hence can be used in molecule detection.

In substitutional doping, the dopant atoms are included in the graphene lattice and thus chemically bonded. Substitutional doping is done via the CVD method using a carbon and dopant source. Substitutional doping opens up many applications in device engineering making graphene a very good candidate as a semiconductor. This study involves the study of transport properties of graphene doped by substitution.

### 1.2.6 Nitrogen (N) Doped Graphene Synthesis (Substitutional)

N-Doped graphene is prepared via a CVD process, using a 25μm thick Cu film on a Si substrate. The substrate is placed in a quartz tube with the flow of hydrogen (20sccm) and argon (100 sccm).[18] When the center of the furnace reaches 800°C, 60 sccm of $CH_4$ and 60 sccm of $NH_3$ is introduced into the flow as C source and N source respectively. The substrate is then moved to high temperature and after 10 min growth; the sample is cooled to room temperature under $H_2$ ambient. Figure 1. 8 shows the growth of N-doped graphene.[18]

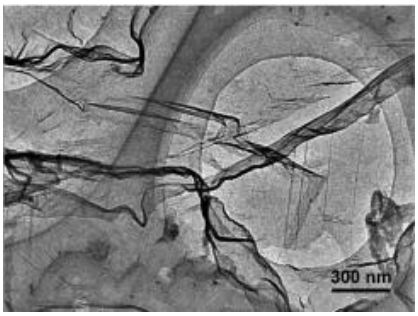


**Figure 1.8** Low resolution TEM image of N-doped graphene. Background is the lacey carbon TEM grid, graphene sheet is crumpled with many ripples.[18]

### 1.3 Structure of Graphene Nanoribbon (GNR)

Graphene Nanoribbons (GNR) are strips of graphene with very thin width of <50nm. GNRs can be terminated in three separate ways called zig-zag (0, n), armchair (m, 0) and chiral (m, n) (Figure1.9), and this termination along the width of the ribbon dictates the size of the band gap.[19]

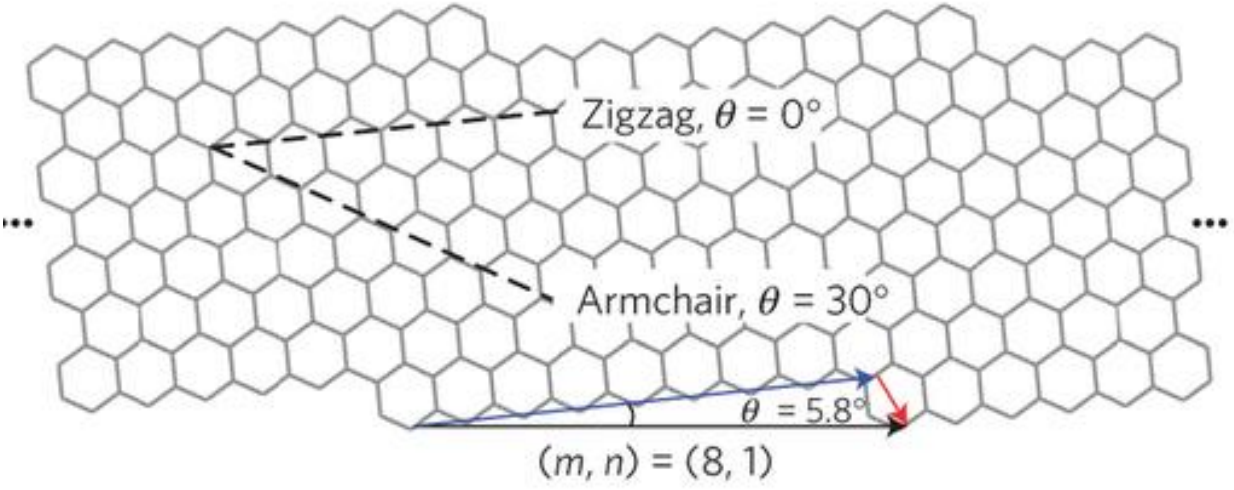


**Figure 1.9** Zigzag and Armchair orientation of Graphene.[5]

Due to their various edge structures, GNRs exhibit different electronic properties ranging from normal semiconductors to spin-polarized half metals, which open the possibility of GNRs as electronic devices.[19]

Within a tight binding approach, (AGNRs) could be metallic or semiconducting depending on their ribbon width; but all zigzag graphene nanoribbons (ZGNRs) are metallic, with a high density of electronic states at the edges. Hence, ZGNRs exhibit characteristic edge effects which are not present in AGNRs. These edge effects, in ZGNR, create a flat band close to the Fermi level making the ZGNR edges more reactive.[19] First-principles calculations show that the GNRs possess a non-zero, direct band gaps. These gaps are small for ZGNR (Figure 1.10) caused due to spin ordering effects at the edges. For AGNRs, the band gap arises from quantum confinement (Figure 1.11) effect that has larger magnitudes than ZGNR.[20]

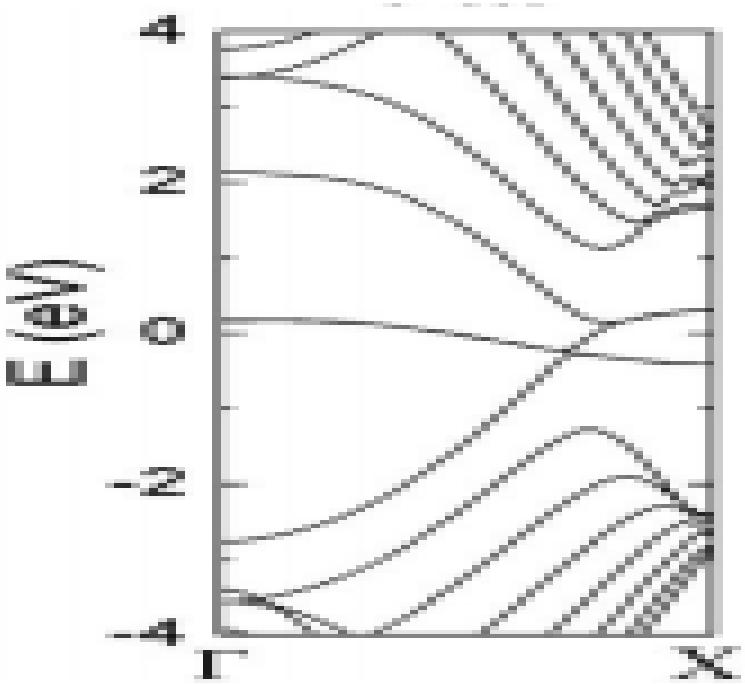


**Figure 1.10** Band structure of ZGNR.

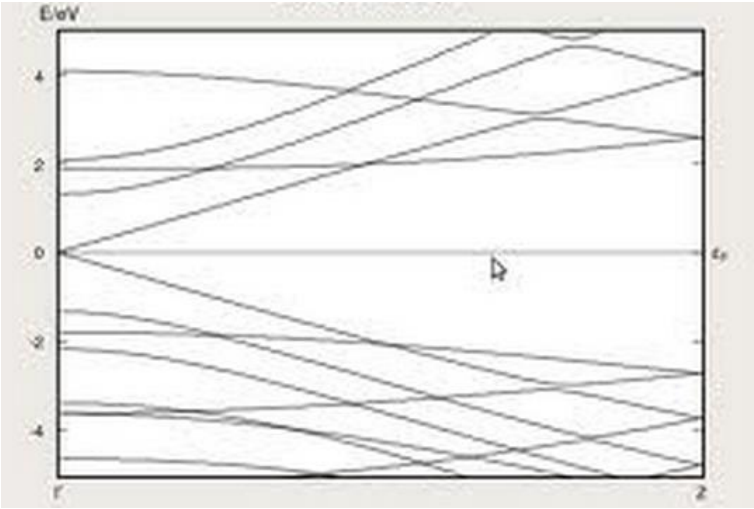


**Figure 1.11** Band structure of AGNR.

For GNRs, the band gap decreases as the ribbon width increases, and in order to create a semiconductor with a desirable band gap, the nanoribbon width should be adjusted accordingly. This property of adjusting the band gap makes graphene an excellent candidate for transistor switching. By applying an electric field, GNR can be altered from an insulator to a conductor. GNRs exhibit very intriguing properties and have become one of the promising candidates for electronic applications.

## 1.4 Overview of Graphene Junction

The invention of p-n junctions date back to 1940s which later resulted in the invention of junction transistors. One of the key technological reasons for success of the p-n junction is mainly due to its ability to locally modulate the energy band gaps via an applied bias.[21]

A graphene p-n junction is created via single layer of graphene in which the carrier type and density in two adjacent regions are controlled by electrostatic gating[8]. For materials with a band gap, the electric field can either switch 'off' the current or rectify it (p-n diode).[22] Being a "gapless" material, the off state is not achievable in

graphene. In order to achieve an off state, the gap can be created by doping graphene with various elements (Group III or Group V). Doping allows p-n junctions to be reconfigurable, using a gate voltage to distinguish between graphene p- n regions within a single sheet. Many researchers have studied the electronic as well as transport properties of doped graphene junctions.

In 2009, Fangping OuYang studied the transport properties of T-shaped graphene junctions using the ATK software and showed that the conductance depends on geometric structures which can be controlled by selective doping.[23] Wei Yao, in 2013, studied the transport properties in graphene p-n junctions and showed that the rectification effect depends on boron doping density and position.[17]

The study of transport properties in graphene p-n junctions is a recent advancement. The thesis discusses transport properties including the current-voltage (I-V) characteristics of doped graphene junctions. Moreover, the software used is similar to the software in use by current researchers since they have produced viable data using ATK.

# CHAPTER 2

# RESEARCH BACKGROUND

## 2.1 Band Structure of Graphene

The unique electronic properties of graphene were first predicted in 1946. Figure 2.1 shows a top view of the hexagonal arrangement of carbon atoms in real space as well as the first Brillouin zone in reciprocal space.

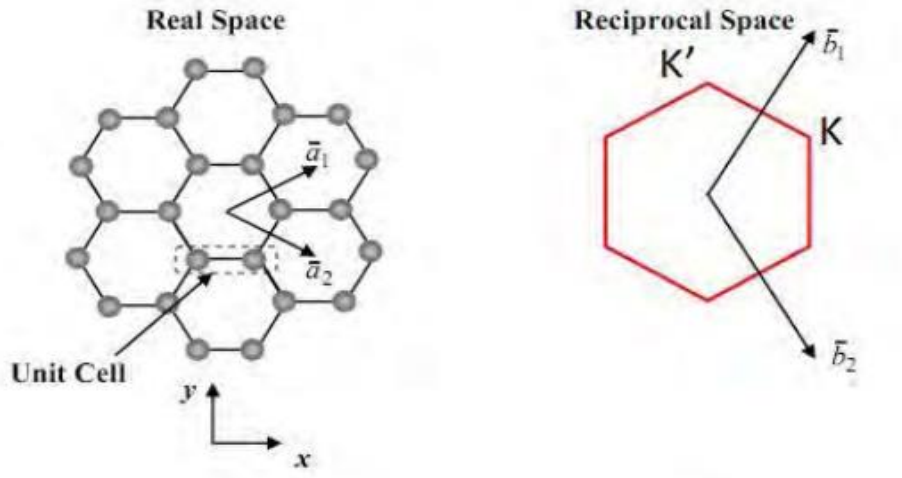


**Figure 2.1** Left. Real space graphene lattice with basis vectors $\overrightarrow{a_1}$ and $\overrightarrow{a_2}$. Right. The first Brillouin zone of graphene in reciprocal space with basis vectors $\overrightarrow{b_1}$ and $\overrightarrow{b_2}$. K and K' are responsible for massless transport at low energy[24].

The real space basis vectors are $\overrightarrow{a_1} = |a_0|(\frac{\sqrt{3}}{2}\hat{x} + \frac{1}{2}\hat{y})$ and $\overrightarrow{a_2} = |a_0|(\frac{\sqrt{3}}{2}\hat{x} - \frac{1}{2}\hat{y})$.

The reciprocal space basis vectors are $\overrightarrow{b_1} = \frac{4\pi}{a_0\sqrt{3}}(\frac{1}{2}x + \frac{\sqrt{3}}{2}y)$ and $\overrightarrow{b_2} = \frac{4\pi}{a_0\sqrt{3}}(\frac{1}{2}x - \frac{\sqrt{3}}{2}y)$

where, the magnitude of the basis vectors is $|a_0| = \sqrt{3}a_{cc}$. The distance between nearest neighbor carbon atoms is $a_{cc}$=0.142nm.

The band structure can be calculated by solving the eigenvalues using the dispersion relation, E($\vec{k}$):

$$E(k) = \pm t\sqrt{3 + 2\cos\vec{k}\bullet\vec{a}_1 + 2\cos\vec{k}\bullet\vec{a}_2 + 2\cos\vec{k}\bullet\vec{a}_3} \qquad (2.1)$$

Transport properties of solids are closely related to the energy dispersion relations, E ($\vec{k}$) in the material and in particular to the behavior of E ($\vec{k}$) near the Fermi level. Graphene is a zero gap semimetal whose specific linear electronic band dispersion near the Brillouin zone corners (Dirac points) gives rise to electrons and holes that propagate as massless Fermions.[25] The valence and conduction bands do not overlap in graphene; they touch at the Fermi Level (Figure 2.2).

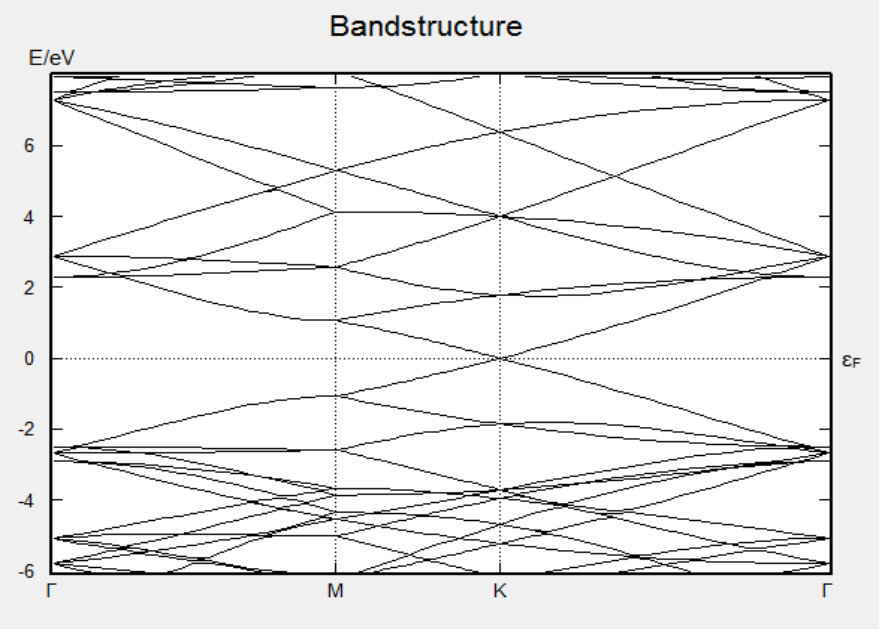


**Figure 2.2** Band structure of a graphene sheet showing a band gap of 0eV.

The low energy properties of graphene can be well described by making a linear expansion of the band structure around the K and K'. This energy can be written as:

$$E(k) = \pm \hbar v_F |k \tag{2.2}$$

where, $v_F$ is the Fermi velocity of $1.10^6$m/s given by,

$$v_F = \frac{1}{\hbar}\frac{\partial E}{\partial k} \tag{2.3}$$

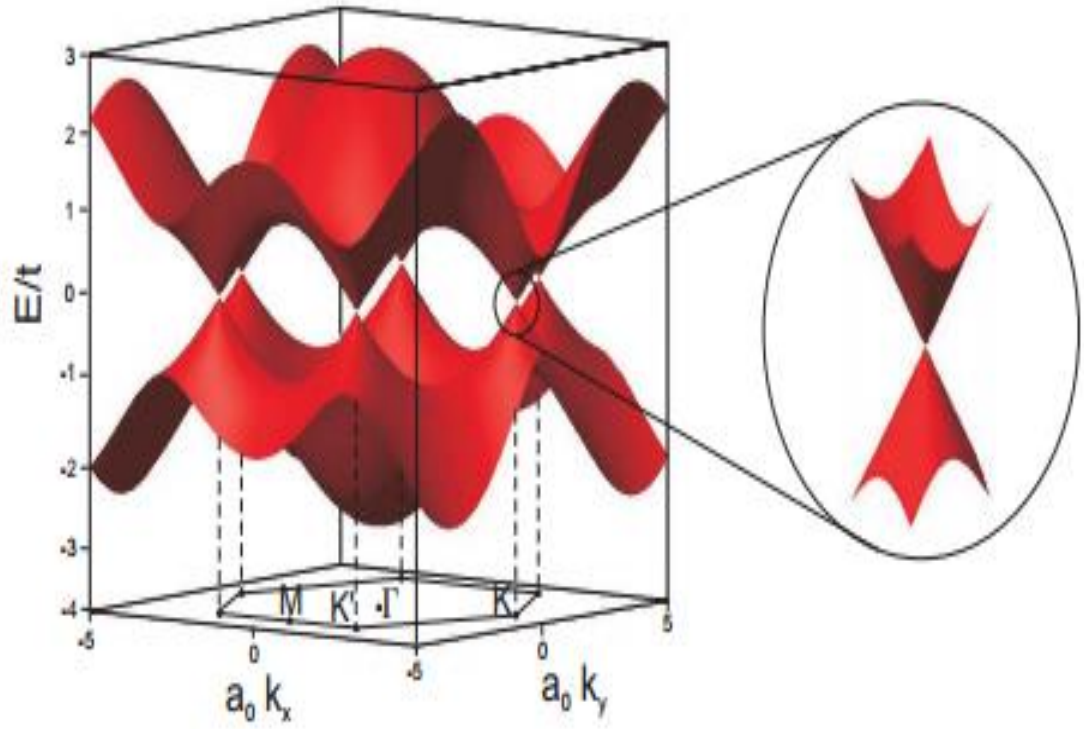


**Figure 2.3** Band structure of graphene calculated with the tight-binding model.[22]

The Fermi surface of graphene consists of double cones with Fermi energy at the intersection of these cones (Figure 2.3). The slope of the band is zero, and hence the effective mass of electrons in that region is zero, which leads to an entirely new transport mechanism in graphene.[26]

## 2.2 Transport Characteristics of Graphene

Transport process usually involves a flow of charge or energy or both. The flow is mainly due to external perturbations such as electric field and temperature gradient. The relationship between forces and flow usually defines various transport coefficients that are the characteristics of electrons and phonons in the material. All modern electronics are based on the ability to control the electronic properties of a material by applying external voltage. This is done by an electric field effect where the gate voltage changes the carrier concentration of the material and consequently its conductivity. The electric field effect in graphene was reported by Novoselov in 2004 and is used in transport measurements.[8]

The electron-phonon interaction in graphene plays an important role in understanding the photoemission spectra observed in graphene. The electric field effect is an alternative method for changing the charge carrier density in low dimensional systems. The electric field effect in graphene, which was first reported by Novoselov et al. in 2004, is widely used as a characterization tool in transport measurements.[25]

The transport characteristics of the material are directly related to the bandstructure of graphene. The carriers in graphene lattice are free to move in two dimensions. In the carrier transport of graphene, the carriers – electrons and holes – close to the Dirac points are of importance. The transport is described by a two component wave function (Equation 2.4) which obeys the 2D Dirac-like equation for massless particles[27].

$$-iv_F\sigma \cdot \nabla\psi(r) = E\psi(r) \tag{2.4}$$

where, σ is the 2D Pauli spin matrix. In the continuum limit, the above (Equation 2.4) corresponds to the effective low energy Dirac Hamiltonian (Equation 2.5)

$$H(k) = \hbar v_F \begin{pmatrix} 0 & k_x - ik_y \\ k_x + ik_y & 0 \end{pmatrix} = \hbar v_F \sigma \bullet k \tag{2.5}$$

The electronic band structure of the energy (E) versus wave vector (k) relation for graphene is given by Equation 2.4.

The two component wave function resembles the spin or wave function of quantum electro dynamics (QED).[27] Corresponding to the spin of particles in QED, the charge carriers of graphene can be attributed with a pseudospin σ. The pseudospin is the direct result of two different carbon sublattices corresponding to the bonding and antibonding combinations.[27]

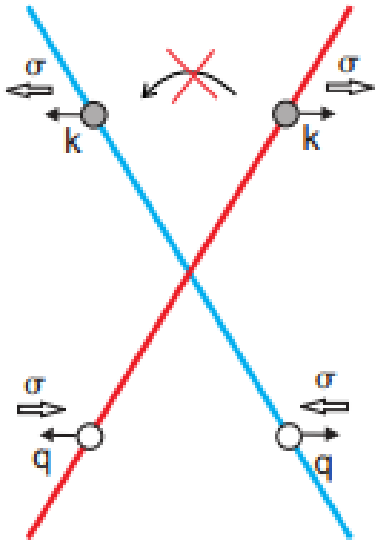


**Figure 2.4** The energy dispersion around the K point.[27]

In Figure 2.4, the red and blue lines correspond to the antibonding and bonding states, respectively. The pseudospin can have two values, either in the direction of or against the momentum. It can be seen that the electrons with energy E travelling in the positive direction originates from the same branch as a hole with energy –E travelling in the negative direction giving it the same pseudospin. This results in suppressed backscattering and Klein tunneling. The back scattering process requires the pseudospin to flip, which is possible in the presence of short range scatters that act differently on sub lattices.[27]

## 2.3 Drude Theory

The classical theory of metallic conductivity was presented by Drude in 1900 and was elaborated by Lorentz in 1905.[28] Drude treated the free electrons as classical ideal gas, meaning the electrons collide with stationary ions and not each other.

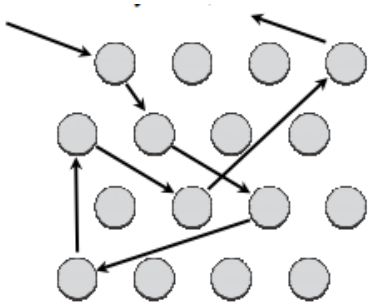

**Figure 2.5** Electrons colliding with stationary ions.[28]

The Drude theory applied the kinetic theory of gases to a metal, considered as a gas of electrons. The basic assumptions made by the Drude theory are:[28]

- When metallic elements are brought together to form a solid, then the valence electrons become freely moving through the metal, whereas the ions remain intact as nearly immobile positive particles.
- Between collisions, the electrons move freely; i.e., there is neither electron-electron interaction nor electron-ion interaction.
- The scattering mechanism leads to instantaneous collisions of the electron with the scatterers.
- The collisions are characterized by a relaxation time $\tau$.
- The electrons achieve thermal equilibrium only through collisions; the velocity after a collision is randomly directed, the speed is as appropriate to the temperature.

With the relaxation time, Drude obtained the electrical conductivity expression, where n is the number of electrons per unit volume.

$$\sigma = ne^2\tau/m \tag{2.5}$$

He also calculated the thermal conductivity and successfully provided the theoretical basis for Wiedemann-Frantz law already established in 1853, which states that

the ratio of electrical and thermal conductivity of any metals is a universal constant at any given temperature.[28]

The Drude theory gives results which are qualitatively correct outside of the quantum Hall regime.[28] In the Drude theory of the electrical conductivity of a metal, an electron is accelerated by the electric field for an average time τ, before being scattered by impurities, lattice imperfections and phonons to a state which has zero average velocity. The average drift velocity of the electron is,

$$v_d = -eE\tau / m \tag{2.6}$$

It is assumed that all electrons drift together and hence the current density,

$$j = -ne\overrightarrow{v_D} \tag{2.7}$$

This Drude theory works well for fields below ~ 0.1T. At stronger fields, the Hall resistivity becomes nearly constant over finite intervals of magnetic fields.[28] The QHE reflects both novel disorder physics as well as novel interaction physics in the quantum Hall regime.

## 2.4 Quantum Hall Effect (QHE)

The discovery of QHE is a remarkable achievement in condensed matter physics. The Hall Effect was discovered by Edwin Hall in 1879.[29] However, the precise quantization of the Hall conductance in units of $e^2/h$ was not recognized until February, 1980. Five years later, in 1985, Klaus von Klitzing was awarded the Nobel Prize in Physics for the discovery of QHE.[29]

The quantum Hall effect occurs in two-dimensional electron systems in the limit of strong perpendicular magnetic field that stems from electronic transport

measurements, where one drives a current *I* through the sample and where one measures both the longitudinal and transverse resistance (Hall resistance). A longitudinal resistance is a resistance measured between two contacts that may be connected by a line which does not connect C1 and C4.[30] Transverse resistance is measured between two contacts connected by an imaginary line connecting C1 and C4 (Figure 2.6a).

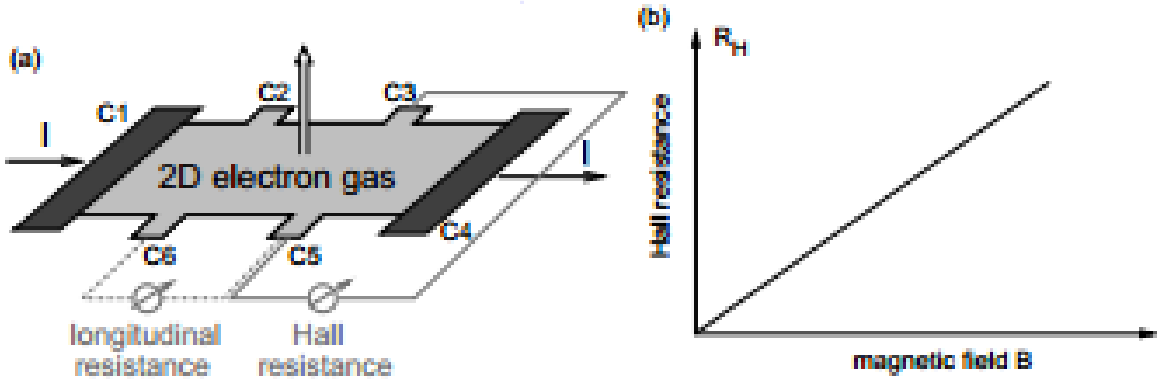


**Figure 2.6** (a) 2D electrons in a perpendicular magnetic field. Logitudinal resistance measured across C5 and C6. Transverse resistance measured across C3 and C5. (b) Classical Hall resistance as a function on the magnetic field.[30]

Due to the existence of quantum Hall effect, it is natural to expect that there exists a classical Hall Effect. Hall showed that the transverse resistance of a thin metallic plate varies linearly with the strength B of the perpendicular magnetic field (Figure 2.6 b):

$$R_H = B/qn_{el} \qquad (2.8)$$

More quantitatively, the classical Hall Effect can be understood within the Drude model for diffusive transport in a metal. Within this model, one considers independent

charge carriers of momentum p described by the equation of motion:

$$\frac{dp}{dt} = -e(E + \frac{p}{m_b} \times B) - \frac{p}{\tau} \tag{2.9}$$

where, E and B are the electric and magnetic field respectively. The macroscopic transport characteristics, i.e., resistivity of the system, are obtained from the static solution of the equation of motion, dp/dt = 0, and one finds for 2D electrons with p = ($p_x$.$p_y$):

$$\begin{aligned} eE_x &= -\frac{eB}{m_b} p_y - \frac{p_x}{\tau} \\ eE_y &= -\frac{eB}{m_b} p_x - \frac{p_y}{\tau} \end{aligned} \tag{2.10}$$

In the above expression, characteristic frequency is visible as,

$$\omega_C = \frac{eB}{m_b} \tag{2.11}$$

This is known as cyclotron frequency as it characterizes the cyclotron motion of a charged particle in a magnetic field.[30] With the Drude theory, the conductivity can be written as:

$$j = -en_{el}p/m_b \tag{2.12}$$

and the mobility can be given as:

$$\mu = e\tau/m_b \tag{2.13}$$

The transport properties in the limit of $\omega_C\tau \to \infty$ are entirely governed in the presence of

a magnetic field by the off-diagonal, i.e., transverse components of conductivity/resistivity.

The theory of quantum Hall effect subjects all physical properties of 2D electron system in the limit where the magnetic field is strong so that the mixing of Landau levels by disorder or electron-electron interaction is considered to be a weak perturbation.[30] This is known as the *quantum Hall regime*. The ratios between the energy scales corresponding to the two interactions are important. The limit where disorder potential is much stronger is referred to as integer quantum hall regime whereas the limit where the interaction potential is much stronger is referred to as fractional quantum Hall regime.

## 2.5 Resistivity and Resistance

The electronic transport, in the framework of the Drude theory, allows for the calculation of conductivity or resistivity of a classical diffusive 2D electrons in a magnetic field.[30] The conductivity and conductance are related to one another but they depend on the geometry of the conductor-the resistance R and hence the resistivity is given by,

$$R = (L/A)\rho \tag{2.14}$$

where, L is the length of the conductor and A is the cross section.

For a d-dimensional conductor, the cross section scales as $L^{d-1}$, such that the scaling relation between the resistance and the resistivity is:

$$R \sim \rho L^{2-d} \tag{2.15}$$

From the dimension point of view, resistance and resistivity are the same in 2D, and the resistance is scale-invariant. Further, the resistance of a 2D conductor depends, in general, on the so-called aspect ratio L/W via some factor f (L/W).[30] However, for transverse Hall resistance, it is the length of the conductor that plays the role of cross

section, such that the Hall resistivity and the Hall resistance truly coincide i.e. f=1. The Quantum Hall effect is highly insensitive to the particular geometric properties of the sample used in transport measurements. Recently, quantum Hall physics experienced the discovery of "relativistic" quantum Hall effect in graphene. The electrons in graphene behave as if they were relativistic massless particles contributing to a very interesting field of research.[30]

## 2.6 Klein Tunneling

Klein tunneling, in which relativistic particles penetrate through a potential barrier without the exponential damping that is characteristic for nonrelativistic quantum tunneling, has never been observed for elementary particles. The tunneling allows transmission of a particle through a potential barrier higher than its kinetic energy, violating the principle of classical mechanics.[30] On the quantum scale, the objects exhibit wave-like characteristics, in which the quanta move against a potential hill described by their wave function. This wave function represents the probability amplitude of finding the object in a particular location. The transmission of the object through the potential hill is termed as tunneling. When E<V then the $\psi(x)$ over V is returned by $\psi'(x)$. In quantum mechanics, an electron tunnels from the conduction into the valence band. Such a tunneling from an electron-like to hole-like state is called as *Klein Tunneling* in which the electron avoids backscattering.

In Figure 2.7, it is shown that an electron hitting a potential barrier is reflected with 100% certainty. In non-relativistic quantum mechanics, the electrons can tunnel through the barrier, but the probability of tunneling exponentially decays with increasing

height and width of the barrier. However, in relativistic quantum mechanics, the barrier gets transparent, even in the limit of infinite barrier height (Klein paradox).[31]

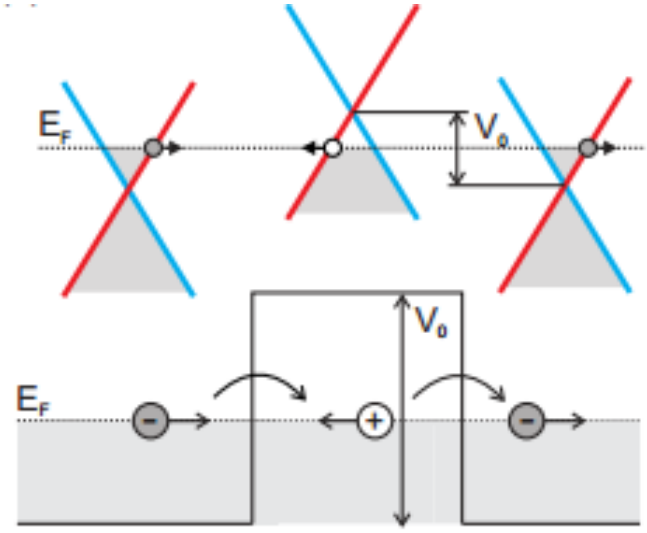


**Figure 2.7** Klein tunneling through an npn barrier.[30]

The Klein paradox in graphene can be understood in terms of electrons and holes. In graphene, the massless carriers behave differently than ordinary carriers (with mass) in the presence of an electric field. A barrier which is repulsive for electrons will be attractive for holes. Since there are hole states inside the barrier with the same energy as the electrons outside, an electron arriving at the barrier can tunnel through it as a hole before leaving again as an electron. Klein tunneling for transport in graphene is that the charge carriers cannot be confined by potential barriers. The Klein tunneling effect has been experimentally observed by Ando in 1998 in which the absence of backscattering (Figure 2.8) is responsible for high conductivity in carbon nanotubes.

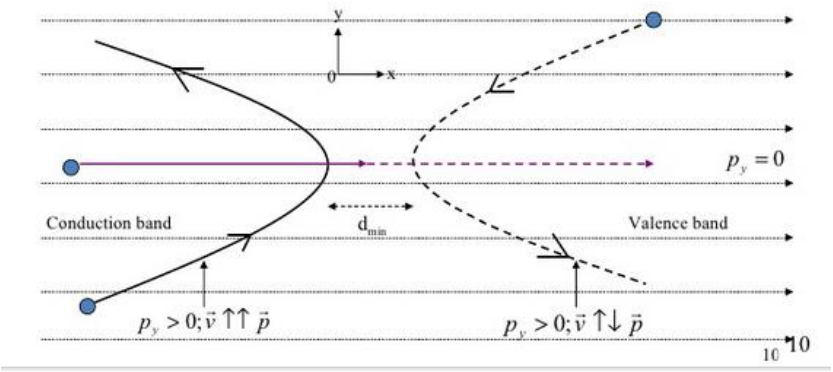


**Figure 2.8** Electron trajectory considering the linear electrostatic potential U(x) = Fx.[30]

The electron is able to propagate through an infinitely high potential barrier since it makes a transition from the conduction band to valence band. In this transition from conduction band to valence band, its dynamics changes from electron-like to hole-like. The equation of motion is thus given by,

$$\frac{d\vec{r}}{dt} = \frac{\delta E}{\delta \vec{p}} = \frac{v^2 \vec{p}}{E - U} \quad \text{at energy E,} \qquad (2.16)$$
$$v^2 \mid \overrightarrow{p^2} \mid = (E-U)^2$$

This shows that, in the conduction band, (U<E) and in the valence band, (U>E). In Klein tunneling, the pairs of electron-like and hole-like trajectories at the same E and $p_y$ have turning points at $d_{min}$ given by $d_{min}=2v|p_y|/F$ (Figure 2.9).

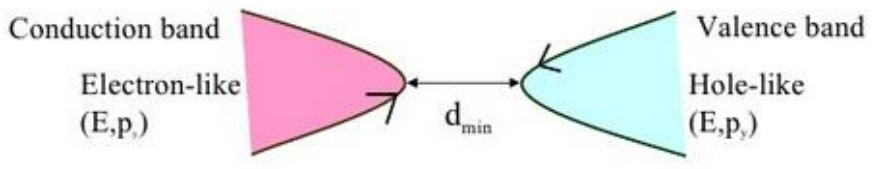


**Figure 2.9** Electron like and hole like trajectories at same E.[21]

The tunneling probability: exponential dependence on $d_{min}$:

$$T(p_y) = \exp(\frac{-\pi |p_y| d_{\min}}{2\hbar}) = \exp(\frac{-\pi v p_y^2}{\hbar F}) \quad (2.17)$$

The applications of the Klein tunneling include Atomic clock, Scanning tunneling Microscope, Tunnel diode, Tunneling transistor and many more.[32] Since graphene exhibits Klein tunneling, it can be very useful to study the transport properties in graphene and use it in such applications.

### 2.7 Quantum Hall Effect in a Graphene

A monolayer graphene shows half-integer quantum Hall effects, where the Hall resistance is quantized at values of:

$$R_{xy} = h / \nu_1 e^2 \quad (2.18)$$

around filling factors,

$$\nu_1 = \pm 4(N + 1/2) \quad (2.19)$$

where, N is an integer, e is the electron charge, h is the Planck's constant and the factor 4 is due to spin and valley degeneracy. QHE in graphene can be observed at room temperature, which is a very intriguing property (Figure 2.10). Graphene reveals significant differences with respect to conventional 2D electron systems. The Landau quantization yields energy levels that disperse differently in graphene as well as particular zero-energy level that is only half filled at the charge neutrality point (v=o).

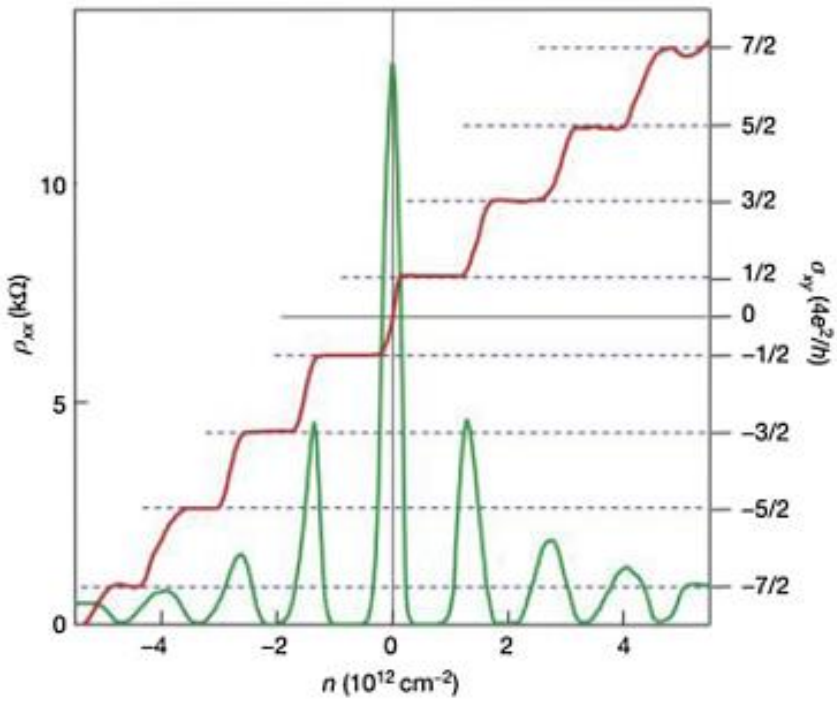


**Figure 2.10** Quantum Hall effect in graphene.[22] The Hall conductivity $\sigma_{xy}$ and the longitudinal resistivity of monolayer graphene as a function of carrier density at B = 14T and T= 4K. This shows half-integer QHE with chiral index J= 1.

The QHE in graphene is not entirely similar to regular QHE, since the charge carriers in graphene are Dirac Fermions. The charge carriers governed by electrodynamics is given by (Equation 2.20), which does not apply for graphene and a QED quantization of graphene electronic band structure is used.

$$En = (n+1/2)\hbar\omega \qquad (2.20)$$

In the presence of magnetic field, the nature of the Dirac Fermions in graphene results in unevenly spaced Landau levels (LL) containing a distinctive LL at the electron-hole degenerating a zero energy given by,

$$E_{n_{MG}^{\pm}} = \pm v_F \sqrt{2ehn_{MG}B} \tag{2.21}$$

The LL levels at high magnetic fields in MG are shown in Figure 2.11.

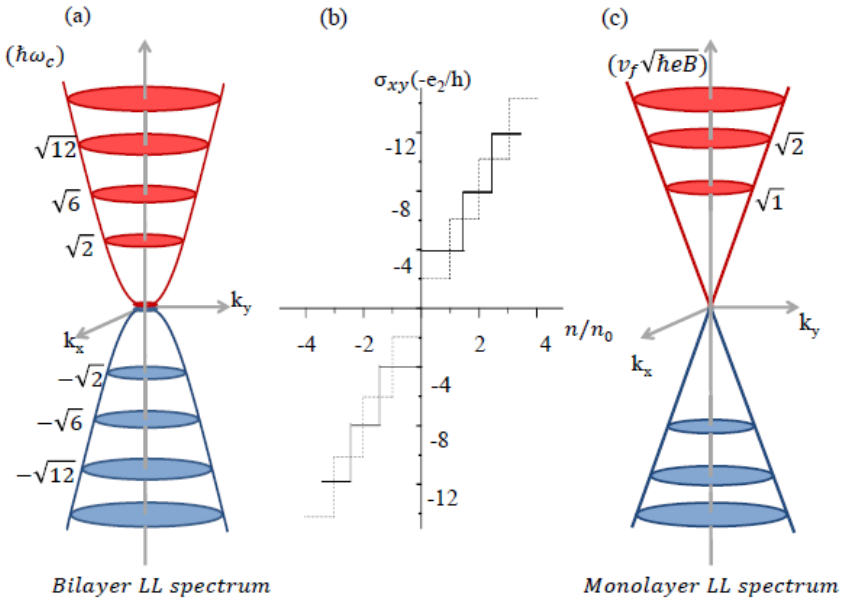


**Figure 2.11** (a) LL for Graphene bilayer (b) Schematics of Hall conductivity as a function of $n/n_0$, for bilayer Graphene (solid line), and monolayer Graphene (dotted line) (c) LL for monolayer Graphene.[33]

It is found that the Hall resistance of a two dimensional electron system has plateaus as a function of the number of electrons at low temperatures and strong magnetic fields.[32] At large B, the Dirac-like energy spectrum of graphene gives rise to a characteristic series of QH plateaus in conductance, reflecting the presence of a zero-energy Landau level, that include only odd multiples of $2e^2/h$ for uniform carrier density in the sheet. These plateaus of QH edge states at the edge of the sheet, circulating in a

direction, are determined by the direction of B and the carrier type.[33] This is why QHE in graphene is known as Half-Integer Quantum Hall Effect.

## 2.8 Thermoelectric Effect

Thermoelectricity refers to a class of phenomena in which a temperature difference creates an electric potential or an electric potential creates a temperature difference. The principle of thermoelectric effect has been known for over 100 years. Recently the practical applications of thermoelectric effect have become more viable.[34]

Thermoelectric effect is the direct conversion of temperature differences to electric voltage and vice versa. Joule heating is the heat generated whenever a voltage is applied across a resistive material. The Peltier-Seebeck effect is reversible whereas Joule heating is not. This effect can be used to generate electricity, to measure temperature to cool objects, or to heat them. Since the direction of heating and cooling is determined by the sign of the applied voltage, thermoelectric devices make very convenient temperature controllers.

### 2.8.1 Seebeck Coefficient

Thomas Johann Seebeck discovered that an emf appears in a circuit composed of two dissimilar metals when the junction between the metals is held at different temperatures.[34] The thermoelectric emf causes a continuous current in the circuit when a complete loop is formed and the current is known as thermoelectric current. This is known as the Seebeck effect.

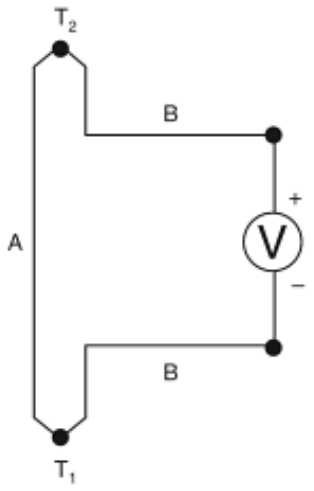


**Figure 2.12** Seebeck Effect.[34]

As long as the two junctions are at different temperatures, the thermoelectric emf exists and the current will keep flowing between the hot and cold junction that are at different temperatures. The Seebeck effect is the conversion of temperature difference directly into electricity. The voltage developed in the circuit, shown in Figure 2.12, is proportional to the difference in temperature between the two junctions and is given by,

$$V = \alpha (T_2 - T_1) \qquad (2.22)$$

This Seebeck effect is observed not only in metals but also in semiconductors. Here, α is known as the Seebeck coefficient. α measures the magnitude of an induced thermoelectric voltage in response to the temperature difference across the material. If the temperature difference ΔT between the two ends of a material is small, then the Seebeck coefficient of a material is written by,

$$\alpha = \Delta V / \Delta T \qquad (2.23)$$

This can be expressed in terms of electric field as,

$$\alpha = E/\Delta T \qquad (2.24)$$

The units of Seebeck coefficient is given as V/K. The higher the Seebeck coefficient value, the better it is since it will create a very large voltage that can be used to provide power.

### 2.8.2 Peltier Coefficient

Peltier effect is the inverse of Seebeck effect involving a junction phenomenon. There is heat absorption or generation at the junctions depending on the direction of current flow. Heat generated by current flowing in one direction is absorbed if the current is reversed. The heat absorbed per second at a junction carrying current I is given by:

$$\text{Heat absorbed in t sec} = \pi_{ab} It \qquad (2.25)$$

Here, $\pi_{ab}$ is the Peltier coefficient and given by H/It. Thus, Peltier coefficient is numerically equal to the applied potential difference expressed in Volts.

Overall, by studying the flow of electrons, the values of Seebeck coefficient and Peltier co-efficient can be estimated. These values determine the various applications of the materials. In this thesis, the Peltier and Seebeck coefficient of the graphene junction and the new applications are discussed.

### 2.9 Early Research – *ab intio* studies

In 2007, Androitis studied that the conducting properties of graphene nanoribbons and junctions are strongly dependent on their size and geometric features.[35] He concluded that there is no conductance for small AZA or ZAZ ribbons (Figure 2.13).

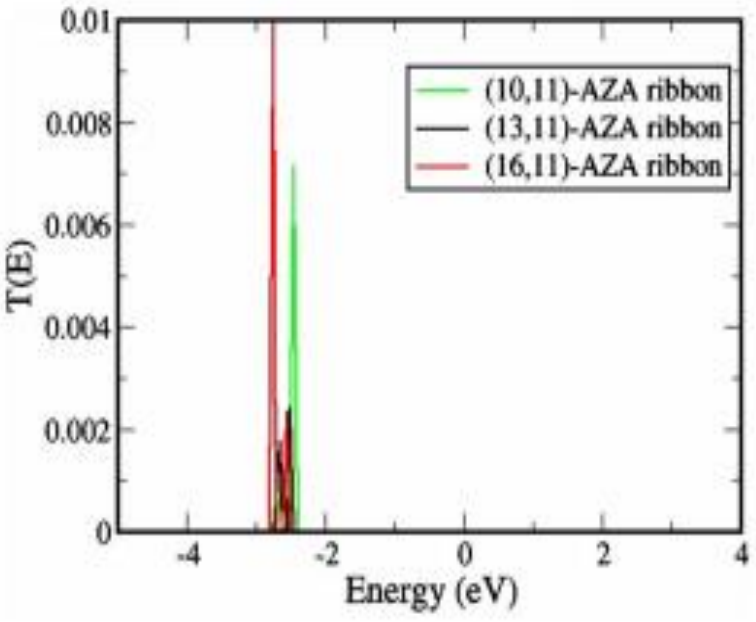


**Figure 2.13** Transmission functions in units of ($2e^2/h$) for AZA structures[35].

Figure 2.13 shows that T (E) exhibits a negligible peak [T (E) = 0.01 in units of $2e^2/h$] at E= -2.25 and 2.50eV. However it was noted that, when the width of the arm type was increased, T (E) at -2.25 and 2.50eV was 0.20.[35]

Later in 2007, Qimin Yan used first principles methods to investigate the Current-Voltage characteristics of GNR Transistors and the effect of edge doping. He showed that GNR field effect transistors can achieve high performance levels with ON/OFF ratios on the order of $10^3$-$10^4$.[36] Figure 2.14 is an I-V curve of AZA GNR-FET connected via armchair metallic leads.[36]

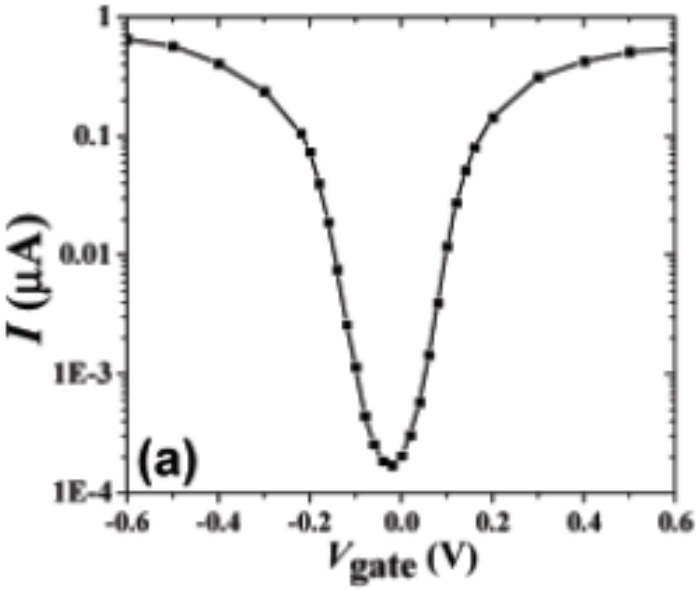


**Figure 2.14** I-V curve for a 5.91nm long channel ($V_{bias}$=20mV).[36]

In 2009, Fangping OuYang demonstrated the intrinsic transport properties and effective B or N doping of the junctions by using first-principles quantum transport simulations. He concluded that the *I-V* characteristics of pure-carbon T-shaped junctions exhibit metallic behavior, and the current in the junction strongly depends on the height of the stem.[23] He reported that the conductance of the devices depends on the geometric structures which can be controlled by selective doping.

In 2012, Wei Yao used the first principle calculations, based on Density Functional Theory (DFT) and Non-equilibrium Green's Function (NEGF), to study the electronic as well as the transport properties of B-doped 6-GNR p-n junction. His results showed that the boron doping interval can influence the rectification effect at low bias and also exhibit Negative Differential Resistance (NDR) phenomena at high positive bias.

# CHAPTER 3

# COMPUTATIONAL DETAILS

## 3.1 Introduction

The physical, chemical, electrical, electronic and optical properties of a solid are determined by their quantized electronic states. The quantum states in low-dimensional systems are produced due to the confinement of the carrier charges in one or two dimensions. Graphene is a conductor; electrons are able to flow through graphene more easily than through even copper. The electrons can travel through the sheet of graphene like mass-less particles, as fast as just one hundredth that of the speed of light. The ways in which electrons behave in graphene make it very helpful to study their fundamental physical properties. Graphene's near perfect crystal lattice provides a very clean system to experiment. By restricting the electrons to only two dimensions, they exhibit some interesting properties such as the 'anomalous quantum Hall effect' and 'Klein tunneling'.

In this chapter, two theoretical concepts used for calculating the electronic structure and the transport properties for graphene are described. These include the Extended Huckel Theory and Non-Equilibrium Green's Function (NEGF) method.

### 3.1.1 Extended Huckel Theory

Erich Hückel was born in Germany on August 9$^{th}$ 1896. He studied mathematics and physics in Berlin. He is best known for his work in the field of chemistry and physics for two contributions: (1). Debye- Hückel theory of electrolytic solutions, (2). Hückel method of approximate molecular orbital calculations on $\pi$ electron systems. In 1930, he published his findings on $\pi$ systems; in 1931, he generalized and expanded the system

theory to explain benzene. Due to his poor communication skills, his findings went unrecognized for over 20 years. It was in 1951 that his 4n + 2 rule was finally clarified by Doering to show if C=C bonds would show aromaticity. Hückel died on February 16th, 1980 with very little worldwide recognition for his contributions to chemistry. Today chemistry students recognize his name and his contributions to the field are quite substantial.

One of the first semi-empirical methods to be developed was Hückel Molecular Orbital Theory (HMO). HMO was developed to describe molecules containing conjugated double bonds. HMO considered only electrons in pi orbitals and ignored all other electrons in a molecule. The Extended Hückel Molecular Orbital Method (EH) was developed out of the need to consider all valence electrons in a molecular orbital calculation.

By considering all the valence electrons, chemists could determine molecular structure, compute energy barriers for bond rotations, and determine energies and structures of transition states for reactions. By considering only the valence electrons, the computed energies could be used to choose between proposed transition states to clarify reaction mechanisms. The total valence electron wavefunction is described as a product of the one-electron wave functions.

$$\Psi_{valence} = \psi_1(1)\psi_2(2)\psi_3(3)....\psi_j(n) \qquad (3.1)$$

where, n is the number of electrons and j identifies the molecular orbital. Each molecular orbital is written as a linear combination of atomic orbitals (LCAO).

$$\psi_j = \sum_{r=1}^{N} c_{jr}\varphi_r,\ j = 1,2...N \qquad (3.2)$$

The energy of the j[th] molecular orbital is given by a one-electron Schrödinger equation using an effective one electron Hamiltonian, $h_{eff}$, which expresses the interaction of an electron with the rest of the molecule:

$$h_{eff}\psi_j = \varepsilon_j \psi_j \tag{3.3}$$

This is the energy eigenvalue of j[th] molecular orbital, corresponding to the Eigen function $\psi_j$. The advantage of using this method is that the exact form of $h_{eff}$ is not required. The total energy of the molecule is the sum of the single electron energies:

$$E_\pi = \sum_j n_j \varepsilon_j \tag{3.4}$$

where, $n_j$ is the number of electrons in orbital j.

In order to use the Extended Huckel method, a set of calculation parameters and approximations must be followed. These parameters include the Basis set, K-point and the Brillouin Zone and lastly the Mesh cut-off.

### 3.1.2 Introduction to NEGF

The Green's function is a function of two space-time coordinates. From the knowledge of this function, one can calculate time-dependent expectation values such as currents and densities, electron addition and removal energies and the total energy of the system. In the absence of external fields, the non-equilibrium Green function method reduces to the equilibrium Green functions. NEGF can be applied to both extended and finite systems. The generic system of NEGF consists of the electron dynamics of the channel described by the Hamiltonian. This channel consists of two contact reservoirs with respective chemical potential $\mu_R$ and $\mu_L$. The NEGF assumes ballistic transport, neglecting self-

energy from scattering. The system is insulated from gate contacts, whose effects are realized via a 3D Poisson solver, which solves for the potential at a given point in real space based on electron density,

$$\nabla^2\phi(\vec{r}) = \frac{q^2}{\varepsilon}[N_D(\vec{r}) - n(\vec{r})] \tag{3.5}$$

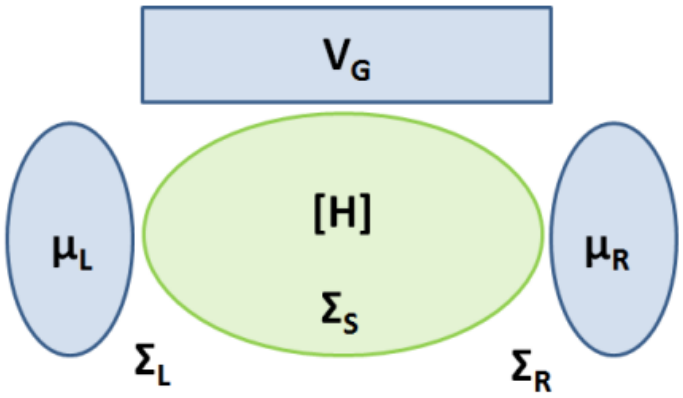


**Figure 3.1** NEGF system

The system is easily expandable to systems with several contacts or gate configurations by adding additional self-energy matrices to NEGF or additional sources to the Poisson solver.

### 3.1.3 Electrostatics

Electrostatic potential is created every time in the presence of a charge density due to an induced electric field. The Poisson's equation correlates the electrostatic potential to charge density as given in Equation 3.6:

$$\nabla^2\Phi(r) = -\frac{\rho(r)}{\varepsilon(r)} = \frac{-q(p(r) - n(r) + N_D(r) - N_A(r))}{\varepsilon(r)} \tag{3.6}$$

where, $\varepsilon(r)$ is the dielectric permittivity of the material, $\rho(r)$, $n(r)$, $N_D(r)$ and $N_A(r)$ are the hole, electron, donor and acceptor concentrations of the system, respectively.

Two types of boundary conditions are usually applied to the Poisson's equation:

- Dirichlet boundary conditions

  $\Phi(0) = F_0$ and $\Phi(L) = F_L$

- von Neumann boundary conditions:

  $$\left.\frac{d\Phi(x)}{dx}\right|_{x=0} = B_0$$

  and

  $$\left.\frac{d\Phi(x)}{dx}\right|_{x=L} = B_L$$

For the transport problems with open boundary conditions, the von Neumann boundary conditions are used assuming that the potential vanishes at the boundary, i.e. $B_0$=$B_L$=0.

The Poisson's equation can hence be discretized on a grid as,

$$\nabla^2\Phi(x) = -\frac{\rho(r)}{\varepsilon(r)} = M \bullet \Phi = -\rho \tag{3.7}$$

where, M is the matrix, $\Phi$ and $\rho$ are vectors containing the discretized values of the electrostatic potential $\Phi$ and charge density $\rho$, respectively.

The Schrödinger and Poisson equations are coupled since $V(x) = -q\Phi(x)$ is used for the Schrödinger to compute $\rho(x)$. This self-consistent loop stops when the convergence is reached.

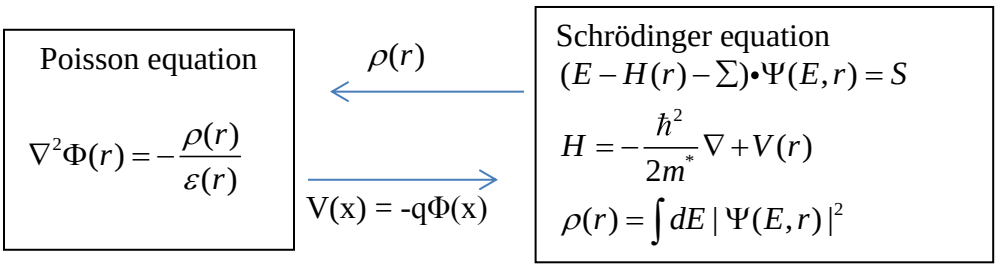


**Figure 3.2** Self-consistent loop.

### 3.1.4 Non-Equilibrium Green's Function

Green's functions are a mathematical construction that are used to solve differential equations subject to specific initial or boundary conditions. They are named after the British mathematician George Green. The 1-D equation of $L(x)f(x)=S(x)$ can be defined by the Green's Function as given below,

$$G(x,x')f(x) = \partial(x - x') \tag{3.8}$$

The general Green's function is given by,

$$f(x) = \int dx' G(x,x') S(x') \tag{3.9}$$

Applying the operator $L(x)$ to the solution $f(x)$ satisfies the original differential equation. The Green's Function $G(x,x')$ is the propagator, which propagates the influence of a perturbation $S(x')$ originally situated at the point $x'$ to the point $x$ at which the function $f(x)$ is evaluated.

The Green's Function $G(x, x')$ can also be a correlation function. If the points $x$ and $x'$ are strongly (weakly) correlated, then $S(x')$ will greatly (poorly) affect $f(x)$.

The Schrödinger equation with open boundaries can be written as,

$$(E - H - \sum) \bullet \phi = S \tag{3.10}$$

Considering, a 1-D and homogenous system, ranging from $x$ =0 to L assuming that Σ=0 and the form of equations is same before and after discretization then,

$$(E + \frac{\hbar^2}{2m^*}\frac{d^2}{dx^2} - V_0) \bullet \phi(x) = S(x) \tag{3.11}$$

The Green's function can hence be computed corresponding to the Schrödinger equation,

$$(E + \frac{\hbar^2}{2m^*}\frac{d^2}{dx^2} - V_0) \bullet G(x, x') = \delta(x - x') \tag{3.12}$$

Due to the delta-function at $x = x'$, a discontinuity is observed and hence the Greens function is evaluated at boundary conditions,

$$G(x, x') = \begin{Bmatrix} A^+ \exp(ik(x - x')) \, \mathrm{x} > \mathrm{x}' \\ A^- \exp(-\mathrm{ik}(\mathrm{x} - \mathrm{x}')) \, \mathrm{x} < \mathrm{x}' \end{Bmatrix} k = \sqrt{\frac{2m^*(E - V_0)}{\hbar^2}} \tag{3.13}$$

By integrating the Schrödinger equation twice and setting the lower and upper integration boundaries to $x = x'$-δ and $x = x'$+δ, the Green's Functions can be written as,

$$\begin{aligned} &G(x' + \delta, x') - G(x' - \delta, x') = 0 \\ &\left.\frac{dG(x, x')}{dx}\right|_{x=x'+\delta} - \left.\frac{dG(x, x')}{dx}\right|_{x=x'-\delta} = \frac{2m^*}{\hbar^2} \end{aligned} \tag{3.14}$$

The coefficient $A^+$ and $A^-$ become,

$$A^+ = A^- = -i\frac{m^*}{k\hbar} \tag{3.15}$$

The Green's Function takes a final form known as Retarded Green's Function and is written as,

$$G(x,x') = -i\frac{m^*}{k\hbar}\exp(ik\,|\,x-x'\,|) \tag{3.16}$$

And the wave function is,

$$\phi(x) = \int dx' G(x,x')\bullet S(x') \tag{3.17}$$

Retarded Green's Function propagates the wave functions generated by a source or perturbation S from its origin at $x'$ to any point $x$.

The retarded Green's Function as discretized Schrödinger equation is written as,

$$(E - H - \Sigma^R)\bullet G^R = I \tag{3.18}$$

The wave function Φ can be calculated from the retarded Green's function and the source vector as,

$$\Phi = \mathrm{G^R}\cdot\mathrm{S} \tag{3.19}$$

Overall, in this section, the Green's function approach in calculating the electron dynamics is reviewed. We defined the self-energy of each part of the system, spectral function and the probability current density; the electric current is derived explicitly using Non Equilibrium Green's function. We will use this formalism to calculate the tunneling phenomena in coupled quantum dots isolated or otherwise.

# CHAPTER 4

# ATOMISTIX TOOLKIT DETAILS

## 4.1 Introduction

Virtual NanoLab (VNL) is a graphical user interface (GUI) that provides a group of modeling tools; the function of these tools involves the set-up, investigation, and the study of nanoscale structures. The quantum mechanical equations are solved by the software by using the advanced software architecture and numerical methods to implement *ab initio* calculations. VNL simulates the electronic structure and calculates the transport properties based on the two systems mentioned earlier, NEGF and Extended Huckel. ATK is the main engine for computing the scripts and hence all the calculations performed in VNL are done by ATK. VNL is a user friendly software as it not only allows creating a script but also helps to set up a virtual experiment.

This thesis involves the use of VNL in order to study the effect of the width and different orientations of the doped atoms. Since the software allows for virtual experiments, it makes it much easier to study the I-V characteristics based on the change in position of atoms.

## 4.2 Device Structure

In this thesis, AZA GNR p-n junction with boron doping (location) was created using the ATK software which is based on NEGF and DFT. Further, the thesis discusses the transport properties and the I-V curve of such junction.

The input format of ATK is NanoLanguage which is an extension to Python scripting language. ATK uses the NEGF system for formalism of simulating device.

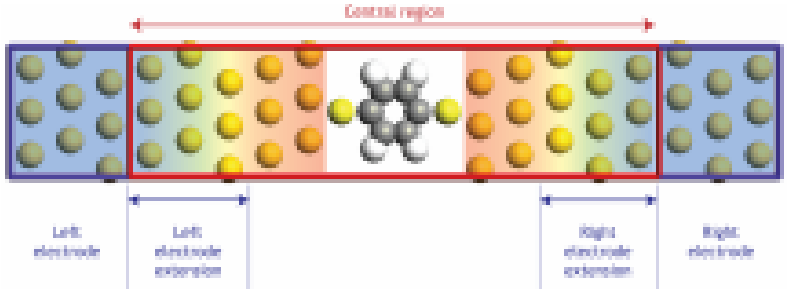

**Figure 4.1** Geometry of device configuration with two electrodes[37].

The system is divided into three parts: left, central and right. The implementation relies on the screening approximation which assumes that the properties of the left and right regions can be decribed by solving a bulk problem for fully periodic electrode cell[37]. This screening approximation is fulfilled when the electrode regions can be described by an equilibrium electron distribution.

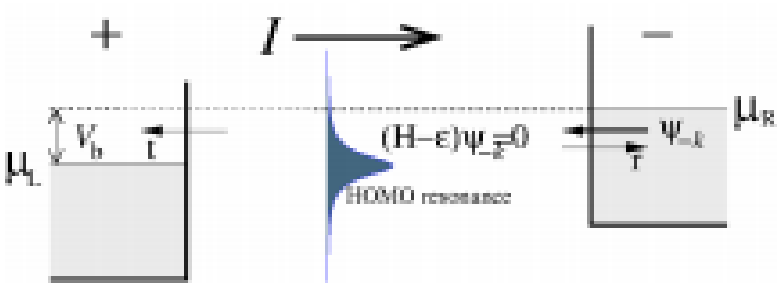


**Figure 4.2** The electron distribution in a device configuration which illustrates a left moving scattering state with origin in right electrode[37].

The system assumes that, in steady state, the electron density of the central region is constant in time, and hence the electron density is calculated independently from each electrode. The electron density is given by the occupied eigenstates of the system:

$$n(r) = n^L(r) + n^R(r) \qquad (4.1)$$

The left and right densities are calculated by summing up the occupied scattering states:

$$n^{L}(r) = \sum_{\alpha} |\psi_{\alpha}(r)|^{2} f\left(\frac{\varepsilon_{\alpha}-\mu_{L}}{kT}\right) \quad (4.2)$$

$$n^{R}(r) = \sum_{\alpha} |\psi_{\alpha}(r)|^{2} f\left(\frac{\varepsilon_{\alpha}-\mu_{R}}{kT}\right) \quad (4.3)$$

The scattering states are usually calculated by first calculating the Bloch states in the electrodes and then solving the Schrödinger equation of the central region using the Bloch state as matching boundary. Instead of using the scattering states, the ATK software uses the NEGF method to calculate the non-equilibrium electron density.

The electron density is given in terms of electron density matrix:

$$D = D^{L} + D^{R} \quad (4.4)$$

The left density matrix is given by NEGF theory,

$$D^{L} = \int \rho^{L}(\varepsilon) f\left(\frac{\varepsilon-\mu_{L}}{k_{B}T_{L}}\right) d\varepsilon \quad (4.5)$$

where,

$$\rho^{L}(\varepsilon) = \frac{1}{2\pi} G(\varepsilon)\Gamma^{L}(\varepsilon)G^{\dagger}(\varepsilon) \quad (4.6)$$

$\rho^{L}(\varepsilon)$ = is the special density matrix.

Also, if there is a non-equilibrium electron distribution in the central region, then the electron distribution in electrode is given by the Fermi function f with an electron temperature $T_L$.

$$G(\varepsilon) = \frac{1}{(\epsilon+i\delta_{+})S-H}; \quad (4.7)$$

G = retarded Green function,

$\delta_{+}$ is an infinitesimal positive number and *S, H* overlap the Hamiltonian matrices.

$$\Gamma^{L} = \frac{1}{i}\left(\sum L - \left(\sum L\right)^{\dagger}\right); \quad (4.8)$$

$\Gamma^{L}$ is the broadening function of the left electrode, given in terms of left electrode self -energy$\sum L$.

### 4.3 Transmission Spectrum Calculations

Once the self-consistent non-equilibrium density matrix has been obtained, the various transport properties of the system can be calculated. One of the most important properties is the transmission spectrum, from which the current and differential conductance can be obtained.

The transmission coefficient in ATK is obtained by the retarded Greens function

$$T(\varepsilon) = G(\varepsilon)\Gamma^{L}(\varepsilon)G^{\dagger}(\varepsilon)\Gamma^{R}(\varepsilon) \quad (4.9)$$

The transmission amplitude of individual scattering states may be obtained through the Transmission Eigenvalues. The "Transmission Eigenvalues" is an analysis which finds the eigenvalues of the transmission matrix.

The transmission matrix at energy E and k-point is given by,

$$T_{nm}(E,k) = \sum_l t_{nl}(E,k)t^{\dagger}_{lm}(E,k) \quad (4.10)$$

where,

$t_{nl}(k)$= transmission amplitude from Bloch state $\psi_n(k)$.

The transmission coefficient is given by the trace of transmission matrix:

$$T(E,k) = \sum_n T_{nn}(E,K) \quad (4.11)$$

Keeping in mind all quantities depend on the quantum numbers parametrically. Transmission eigenvalues sum up to the transmission coefficient:

$$T = \sum_\alpha T_\alpha \quad (4.12)$$

### 4.4 Calculating the Current

Current is calculated from the transmission coefficient using:

$$I(V_L V_R T_L T_R) = \frac{e}{h}\sum_{\sigma}\int T_{\sigma}(E)\left[ f\left(\frac{E-\mu_R}{k_B T_R}\right) - f\left(\frac{E-\mu_L}{k_B T_L}\right)\right] dE \qquad (4.13)$$

where, *f* is the Fermi function, $T_{R/L}$ is the electron temperature of the right or left electrode and $T_{\sigma}(E)$ is the transmission coefficient for the spin component σ.

The chemical potentials of the left and right electrode, given by $\mu_{R/L} = E_F^L - eV_{R/L}$, are defined relative to the Fermi level of the left electrode. These chemical potential are related to the applied bias and hence $\mu_R - \mu_L = eV_{bias}$; therefore, $V_{bias} = V_L - V_R$.

The transmission spectrum itself is usually rather insensitive to temperature and is used in self-consistent calculations, but often depends strongly on the electrode voltages. Thus, for an accurate estimate of the current, the transmission spectrum should be calculated self-consistently for each desired bias.

ATK uses very precise method to calculate the transport properties of the system. Transmission spectra, for various concentrations of boron doped graphene p-n junctions, are generated in this Chapter and various coefficients such as Seebeck, Peltier, and Conductance are calculated.

### 4.5 Calculating Transport coefficients

The linear response transport coefficient of an applied voltage difference or temperature difference between the two electrodes is given by,

Conductance:

$$G_e = \frac{dI}{dU} \mid \mathrm{dT} = 0 \tag{4.14}$$

Peltier coefficient:

$$\Pi = \frac{I_Q}{I} \mid \mathrm{d} = 0 \tag{4.15}$$

Seebeck coefficient,

$$S = -\frac{dU}{dT} \mid I = 0 = \frac{\Pi}{T} \tag{4.16}$$

These linear response coefficients are calculated by the Transport Coefficients. To perform these calculations, the ATK uses the Electron Transmission Spectrum.

# CHAPTER 5

# RESULTS AND DISCUSSION

## 5.1 Band Structure Analysis

The electronic bandstructure of GNR, both doped and undoped, are discussed in this chapter.

The armchair configuration of Pristine GNR (PGNR) has a band structure that is dependent on its width. This is explained by the fact that the sheet itself acts like a potential well where the electrons are confined to form standing waves along Cr, the rolling vector, albeit with slightly different boundary conditions. ($Cr = m*a_1 + n*a_2$, where, m and n are integers and $a_1$ and $a_2$ are the unit cell vectors of graphene lattice.) In a GNR, the two nodal points of the standing wave must be at the ribbon edge, while in a Single wall nanotube (SWNT), they can be anywhere, i.e., a circumferential periodic boundary condition.

(a) (b)

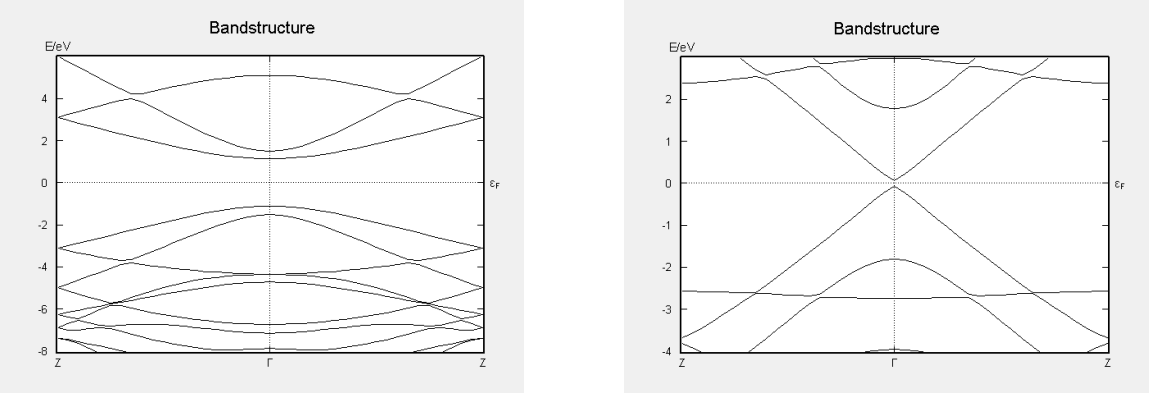


**Figure 5.1** Bandstructure of AGNR widths (a) 4 atoms (b) 5 atoms.

(a) (b)

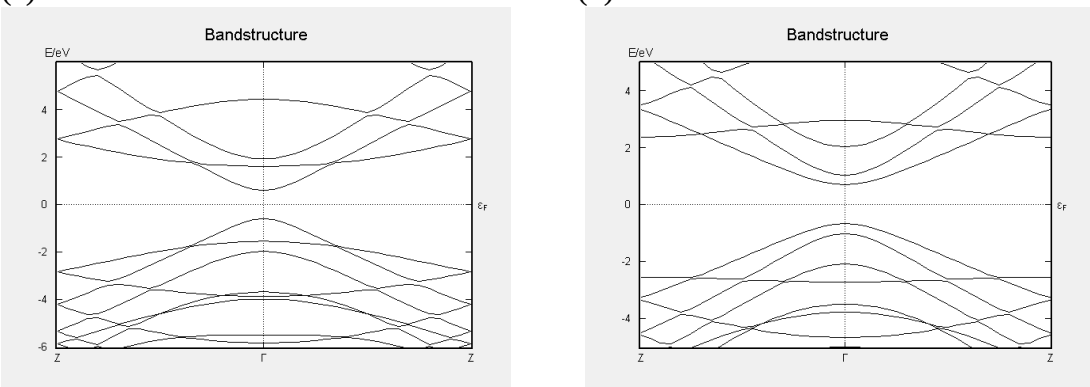


**Figure 5.2** Bandstructure of AGNR widths (a) 6 atoms (b) 7 atoms.

(a) (b)

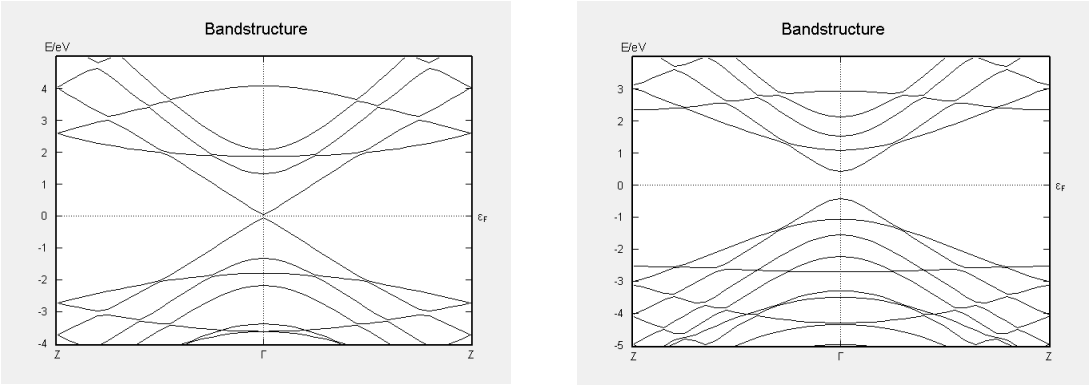


**Figure 5.3** Bandstructure of AGNR widths (a) 8 atoms (b) 9 atoms.

(a) (b)

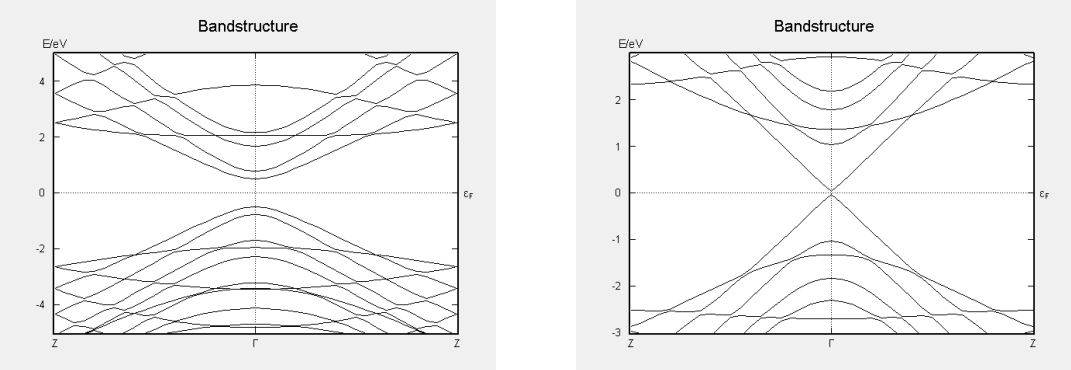


**Figure 5.4** Bandstructure of AGNR widths (a) 10 atoms (b) 11 atoms.

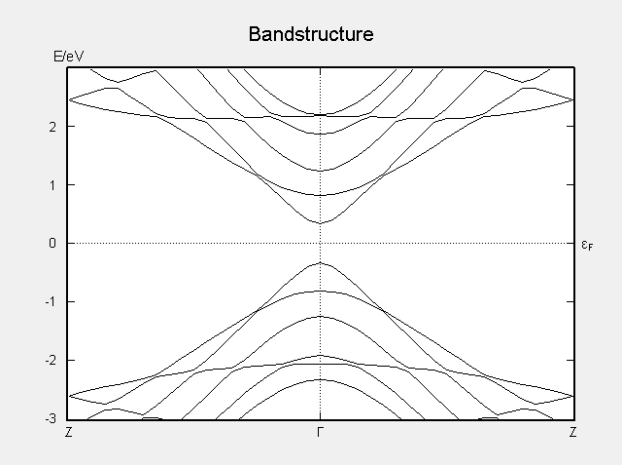


**Figure 5.5** Bandstructure of AGNR with a width of 12 atoms.

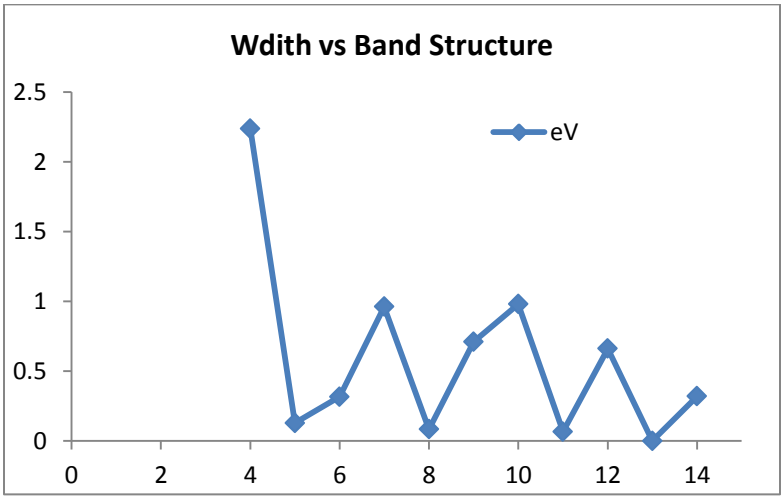


**Figure 5.6** Variation in band gaps as the width (number of atoms) varies.

The band structure of 12 Atom AGNR is close to that of Ge (0.626 eV). The actual width of this nanoribbon is about 2.5 nm. 12 AGNR has been fabricated successfully and doped with various dopants. Hence the 12 Atom AGNR has been chosen to study the transport properties.

A junction is created using ZGNR and AGNR. To maintain the consistency in the device analysis, it is imperative that the band structure of ZGNR is also calculated. From the simulation, it is evident that ZGNR-AGNR-ZGNR junction configuration displays the Metal –Semiconductor-Metal configuration that is addressed in this work. The Fermi Level in all the Z-GNR nanoribbons of widths 4-12 lies within the conduction band.

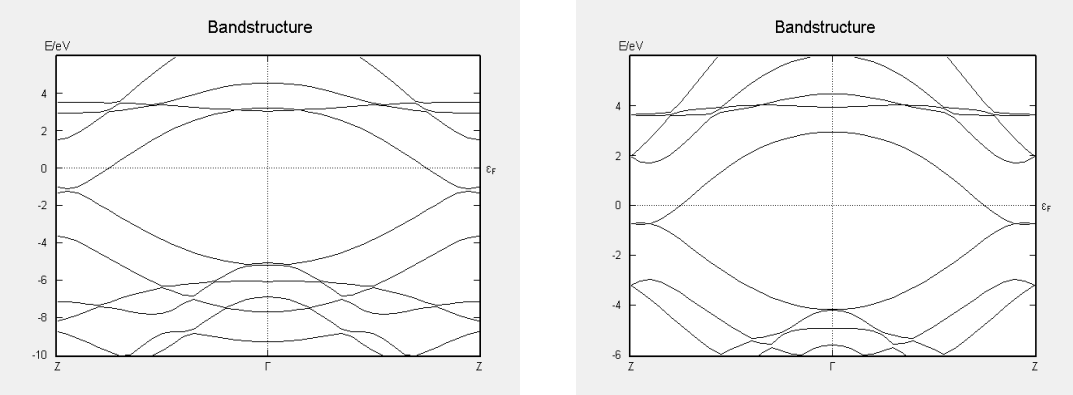


**Figure 5.7** Band structure of ZGNR width (a) 4 atoms (b) 6 atoms.

(a) (b)

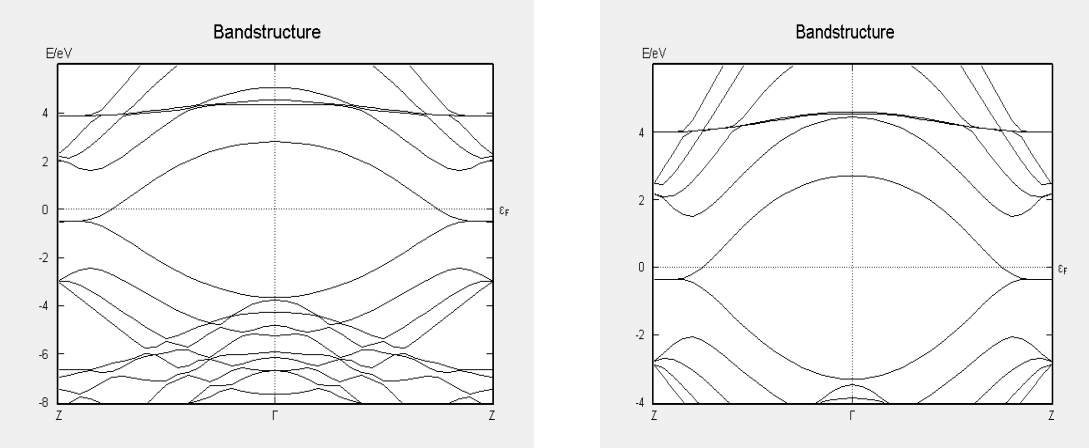


**Figure 5.8** Band structure of ZGNR width (a) 8 atoms and (b) 10 atoms.

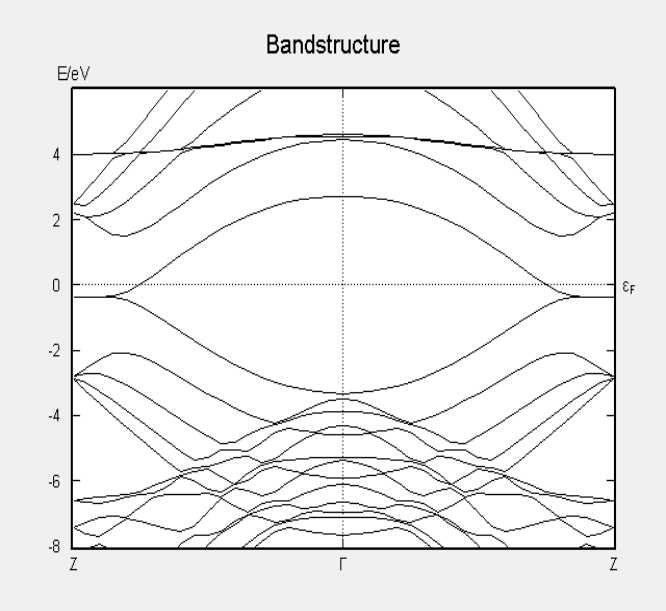


**Figure 5.9** Band structure of ZGNR with a width of 12 atoms.

In order to create viable junction that would show transistor properties, doping of the semiconductor part is necessary. The 12 atom AGNR is doped with boron (p-type) and nitrogen (n-type) - (Figure 5.10a) 4 % N doped; (Figure 5.10b) 4% B. In both cases, the impurities lie on the edge of the atoms. For 2% nitrogen doped GNR, with the

impurities lying in the center of the ribbon, the Fermi level is found to be in the conduction band, as shown in (Figure 5.10c); (Figure 5.10d) shows the position of N with respect to the edge. A very clear departure from the expected (the valence band extending above Fermi level) is shown in (Figure 5.10a).

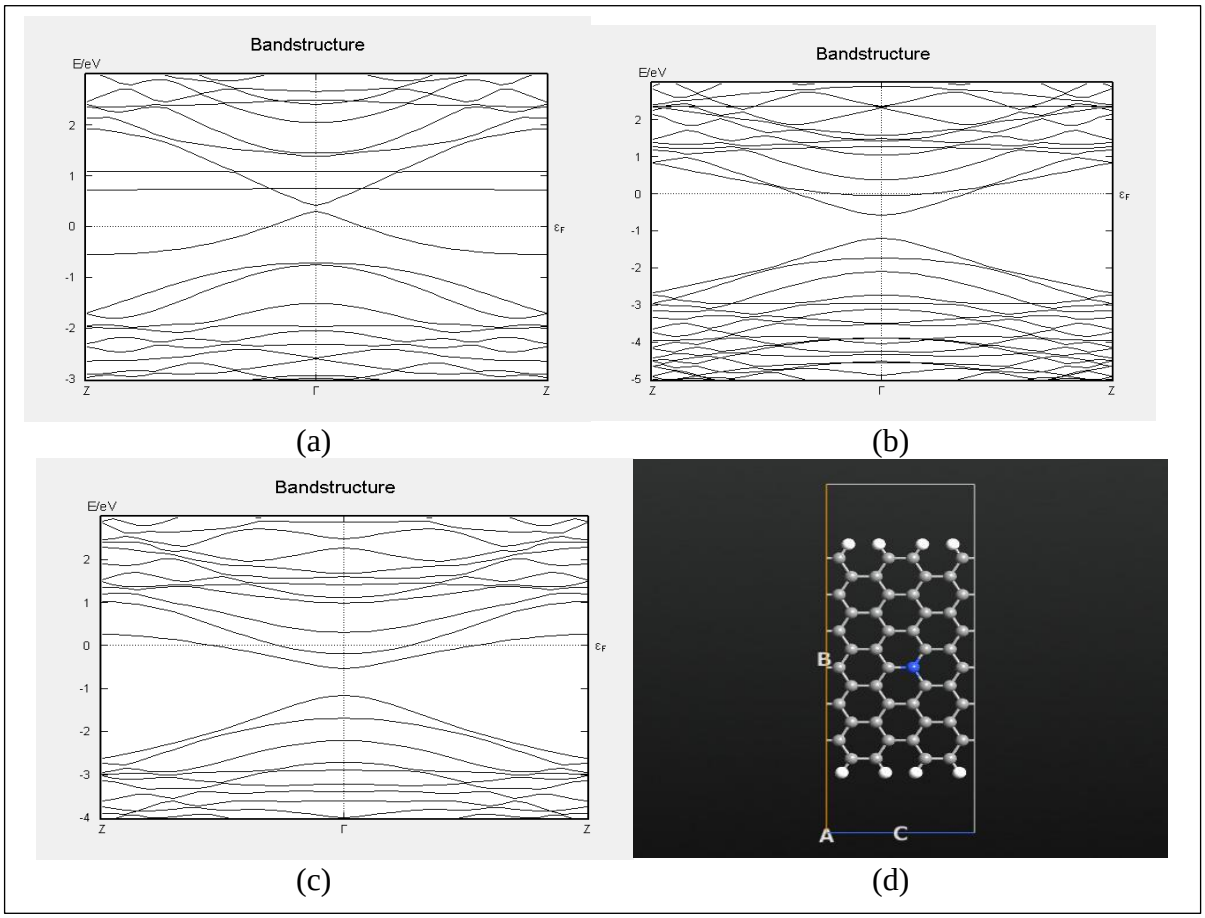


**Figure 5.10** Band structures of Doped AGNR (a) 4% N Doped (b) 4% B Doped (c) 2% N Doped (d) position of Nitrogen from (c).

### 5.2 I-V Characteristics of GNR junction

In pristine graphene, the chirality determines the conductivity as seen from the I-V curves for various widths. At certain widths, the semiconducting properties are more pronounced. These widths determine the wavelengths of the standing waves, which, in turn, determine the sub-band locations in the E-k plot. When the biasing potential exceeds 0.12V, the I-V curve shows linearity. In case of the 8-atom wide PGNR, the band gap is about 0.3 eV and it is evident from the I-V plot that the On-State is + 0.33 V. The band gap of 10-atom and the 4-atom wide PGNR is large enough to show semiconducting properties

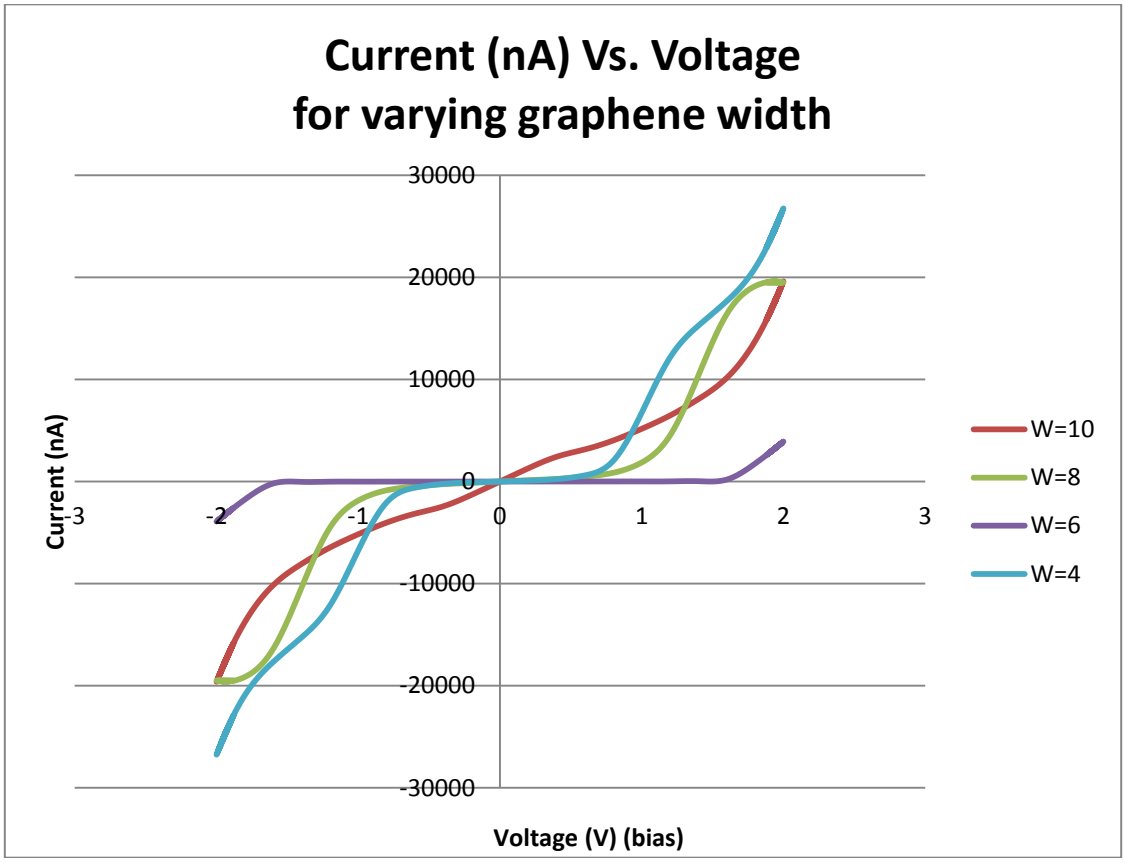


**Figure 5.11** Current Vs Voltage graph for varying graphene width showing conductivity.

The ZAZ GNR Configurations show the properties of a semiconductor junction. The 12 atom ZAZ structure is studied for its I-V characteristics. In this Chapter, undoped, B-doped, N-Doped, B and N Doped (P-N Junction) ZAZ junctions are simulated.

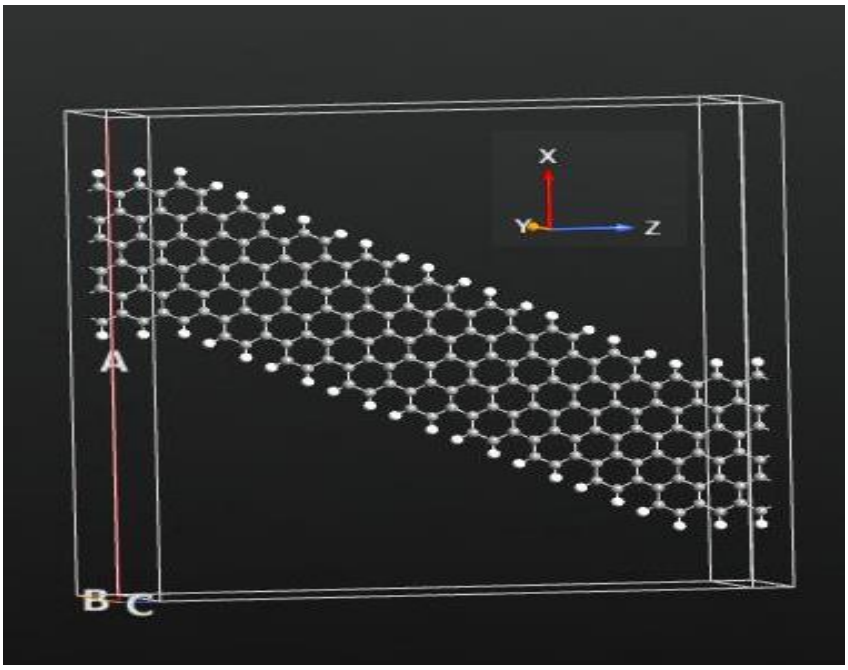


**Figure 5.12** ZAZ GNR junction device.

The boron doped ZAZ junction I-V characteristics are shown below (Figure 5.13). The impurity concentration is 2 % and 4 %. Various device configurations are studied.

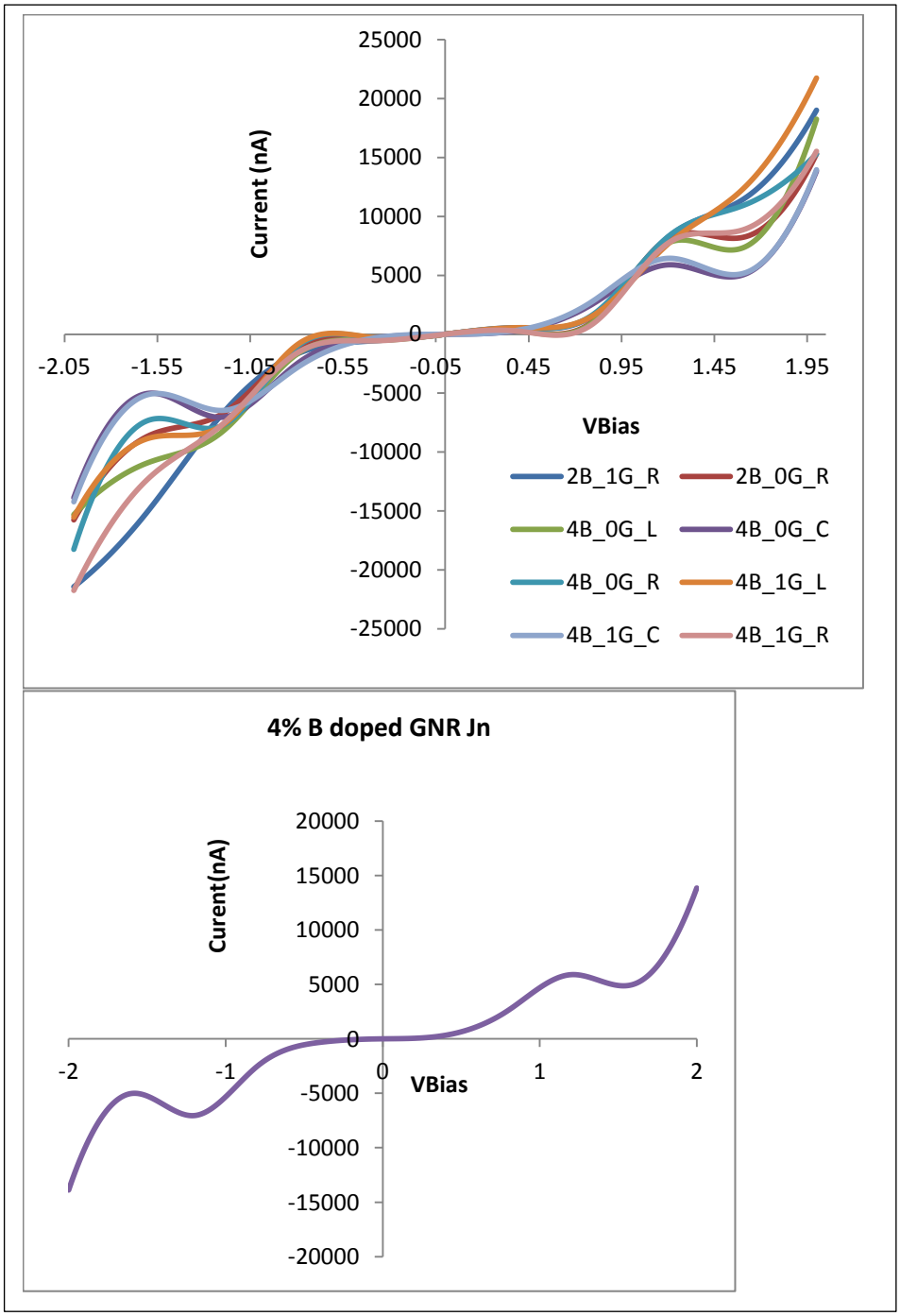


**Figure 5.13** I-V curve of Boron Doped ZAZ junction.

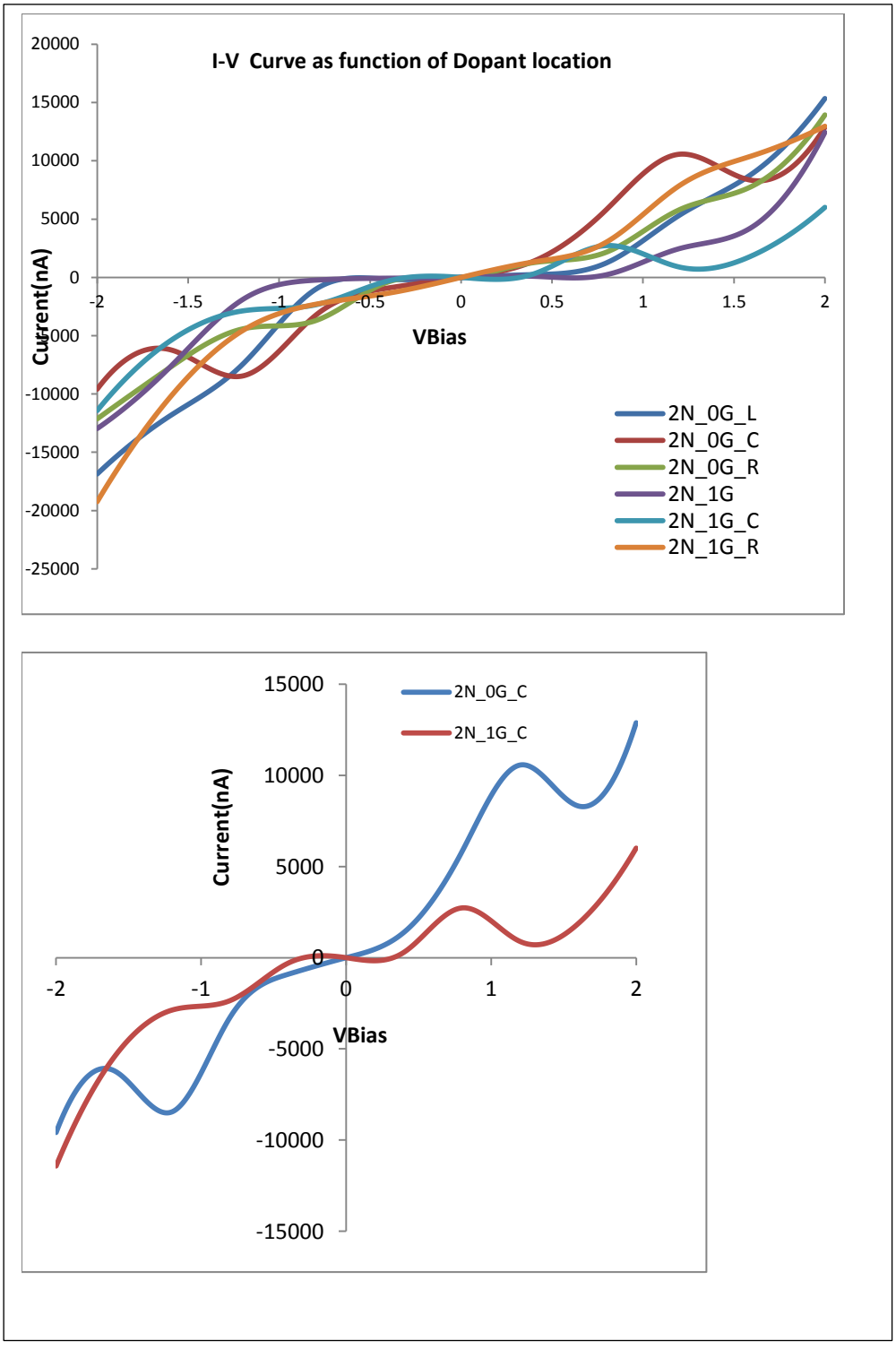


**Figure 5.14** I-V curve of Nitrogen Doped ZAZ.

Figure 5.13 and Figure 5.14 show the I-V characteristics of the GNR junction doped with 2% boron and nitrogen, respectively. The location of N and B is at the central region of the edge of the GNR. Both B doped and N doped GNR Junctions show significant Negative Differential Resistance (NDR). This is more pronounced in case of nitrogen doping. Another interesting observation is increasing ohmic nature with the change in location of the dopants. Nitrogen doped device configuration exhibits a pronounced semiconductor behavior and the NDR effect is observed to be minimal.

### 5.3 Thermoelectric Properties

In this study, the thermoelectric properties were simulated for the GNR Junctions that displayed high NDR effect. The variation in the Peltier coefficient with temperature is shown as function of doping.

When the concentration of nitrogen increases, the dimensionless Figure of Merit, ZT, seems to decrease considerably. This is mostly explained by the decrease in both conductivity and mobility of the electrons.

$$ZT = S^2\sigma T/k \tag{5.1}$$

where, S is the Seebeck coefficient, $\sigma$ is the electrical conductivity, T is the absolute temperature and k is the thermal conductivity.

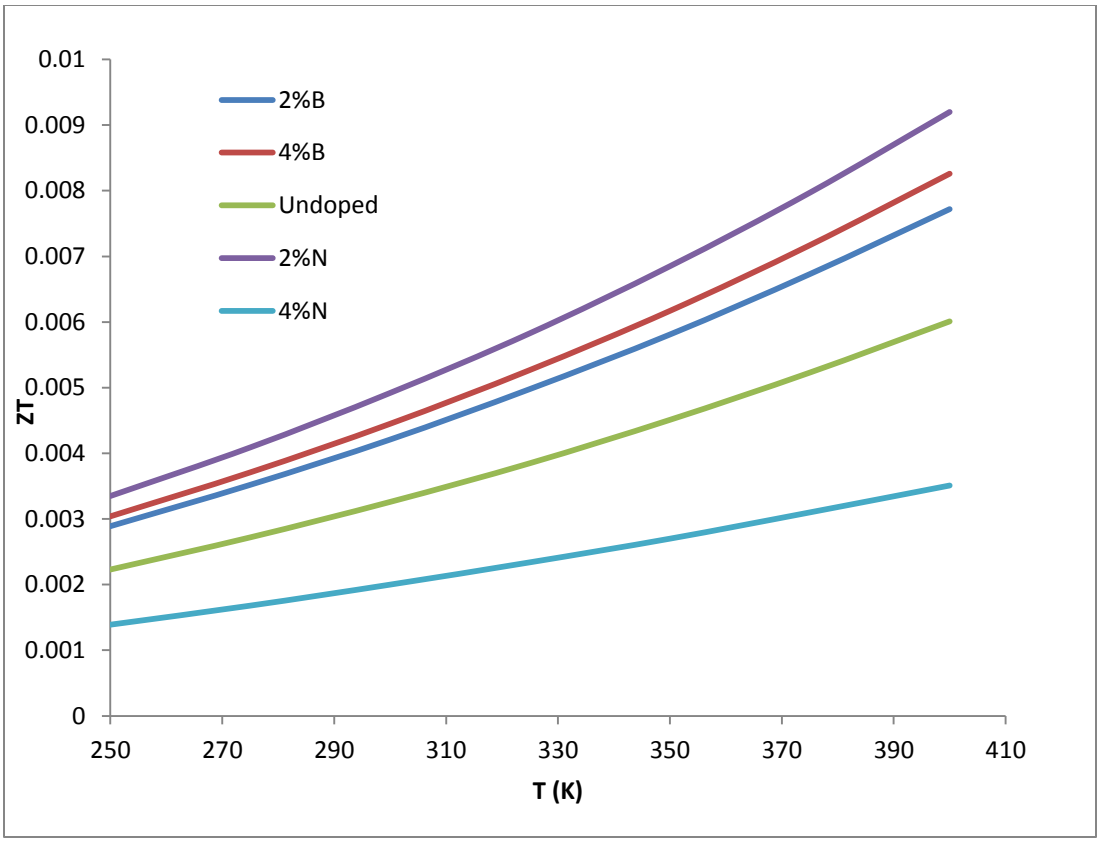


**Figure 5.15** Variation of Peltier coefficient with temperature as function of doping.

Figure 5.15 shows the maximum Peltier coefficient for 2% boron. This is explained by the scattering by boron and the associated smallest mean free path.

# CHAPTER 6

# CONCLUSIONS

Graphene ZAZ junctions exhibit varying properties depending on the various structural configurations. In this thesis, it was found that the transport properties of graphene depend on their width, the edge of GNR, doping concentration and the type of dopant used. The calculations of the band structure contributed towards the determination of the minimum length of GNR required for studying the transport properties. The minimum length had a band gap equivalent to that of germanium and hence the importance of the width being 12 atoms wide. This band gap indicated fluctuating changes when doped with elements such as B and N. The viable junction showing transistor properties was hence created by doping the semiconductor part of ZAZ. By doping, the I-V characteristics were studied which showed significant NDR which was more pronounced in the case of nitrogen. Also, the changing positions of the dopants contributed towards the I-V curve to be more ohmic. The edge doping caused minimum NDR and semiconductor behavior as compared to central doping. Lastly, the thermoelectric properties were studied - the increasing concentration of N causes the Figure of Merit to decline due to the decrease in conductivity as well as mobility of electrons.

## REFERENCES


1. Wikianswers What makes carbon unique. http://wiki.answers.com/Q/What_makes_carbon_so_unique (22 November),

2. Kopeliovich, D. D. Graphite. http://www.substech.com/dokuwiki/doku.php?id=graphite (11/28),

3. Barbier, M. Transport properties of nanostructures and superlattices on single layer and bilayer graphene University Antwerpen, Antwerpen, 2012.

4. Shylau, A. Electron transport, interaction and spin in graphene and graphene nanoribbons. Linkoping, Norrkoping, 2012.

5. Hass.J., R. F., T. Li, X. Li, Z. Zong, W. A. de Heer, P. N. First, E. H. Conrad, C. A.Jeffrey, and C. Berger *Applied Physics Letters* **2006,** 89, (14), 143.

6. Jones, A. Mechanical Exfoliation to Make Graphene and Visulization. http://carbon.chem.wisc.edu/Files/MechanicalExfoliation.pdf (18 October),

7. Anteroinen, J. Structural and Electrical Characteristics of Graphene Field Effect Transistors. AALRO school of Electrical Engineering, AALTO, 2011.

8. Novoselov .K. S., A. K. G., * S. V. Morozov,D. Jiang,Y. Zhang, S. V. Dubonos, I. V. Grigorieva, A. A. Firsov. *Science* **2004,** 306, (22).

9. Kosynkin D., A. L. H., A. Sinitskii, J. R. Lomeda, A. Dimiev, K. B. Price, and J. M. Tour. *Nature* 458, 876.

10. Yi, Z., Luyao Zhang. *Accounts of chemical research* 46, (10), 2339.

11. Eizenberg, M. B., J.M. **1979,** 82, 236.

12. Yu, Q. K. L., J.; Siriponglert, S.; Li, H.; Chen, Y. P.; Pei, S. S. *Applied Physcis Letters* **2008,** 93, (113103).

13. Li, X. C., W.; An, J.; Kim, S.; Nah, J.; Yang, D.; Piner, R.; Velamakanni, A.; Jung, I.; Tutuc,E.; Banerjee, S. K.; Colombo, L.; Ruoff, R. S. *Science* **2009,** 324, 1314.

14. Schaefer, H. E., *Nanoscience*. Springer: Berlin, 2010.

15. Levente Tapasztó, G. D., Philippe Lambin & László P. Biró. *Nature Nanotechnology* **2008,** 3, 401.

## REFERENCES


16. Dacheng Wei, Y. L. *Advance Materials* **2010,** 22, (30), 3241.

17. Wei Yao, K. L. Y., G.Y.Gao. *Elsevier Solid State Communications* **2013,** 153, 52.

18. Dacheng Wei, ‡ Yunqi Liu,*,† Yu Wang,† Hongliang Zhang,†,‡ Liping Huang,†,‡; Yu†, a. G. *NanoLetters* **2009,** 9, (5), 1758.

19. Nakada K., M. F., G. Dresselhaus, and M. S. Dresselhaus. *Phys.Rev.B* **1996,** 54, (9858).

20. Son Y W, C. M. L. a. L. S. G. *Phys.Rev.Lett* **2006,** 97, (216803).

21. Raza, H., *Graphene Nanoelectronics*. Springer: 2012.

22. Ryan, W. J. Electronic Transport in Graphene p-n junctions, Short Noise, and Nanoribbons. Harvard University, 2009.

23. Fangping OuYang, J. X., Rui Guo, Hua Zhang and Hui Xu. *Nanotechnology* **2009,** 20, 6.

24. Guo, J. Carbon nanotube electronics:Modeling, physics and applications. Purdue University, West Lafayette, IN, 2005.

25. Motta C., S. S.-P., M.I.Trioni. *cond-mat.mes-hall* **2012,** 7.

26. B. P. Growing Graphene via Chemical Vapor Deposition. Ponoma College, Ponoma, 2011.\

27. Zurich.E. Transport properties of three-terminal graphene devices. University of Science and Technology, Norway, 2008.

28. Uichiro M.Introduction to the electron theory of metals.

29. Robert. Laughlin, H. S. Additional background material on the Nobel Prize in Physics 1998. (4/10),

30. Mark.Goerbig Quantum Hall Effects. (11/15/2013),

## REFERENCES


31. Zurich, E. Transport properties of three-terminal graphene devices. Norwegian University of Science and Technology, Norway, 2008.

32. Deepak, R. *Klein Tunneling* University og Tennessee Space Institute: Tennessee, 2011.

33. Williams J.R., L. D., C.M.Marcus Quantum Hall Effect in a Gate-Controlled p-n Junction in Graphene. (11/2/2013),

34. Avadhanulu M.N., P. G. K., *A Textbook of Engineering Physcis for B.E, B.Sc (Engg)*. S.Chand: New Delhi, 1992.

35. Andriotis, A. *Applied Physics Letters* **2007,** 91, (152105).

36. Qimin Yan, B. H., † Jie Yu,† Fawei Zheng,† Ji Zang,‡ Jian Wu,†; Bing-Lin Gu, F. L., *,‡ and Wenhui Duan*,†. *NanoLetters* **2007,** 7, (6), 1473.

37. Soler J. M., E. A., J. D. Gale, A. García, J. Junquera, P. Ordejón, and D. Sánchez-Portal, J. *Phys. Condens. Matter* **2002,** 14, 2745